Bidirectional Control of Parathyroid Hormone and Bone Mass by Subfornical Organ

Lu Zhang[1, 2 #], Nian Liu[1, 2, 3 #], Jie Shao[1], Dashuang Gao[1], Yunhui Liu[1], Di Chen[4], Liping Wang[1], William Weijia Lu[2,*], Fan Yang[1,*]

[1]The Brain Cognition and Brain Disease Institute, Shenzhen Institute of Advanced Technology, Chinese Academy of Sciences, Shenzhen, China

[2]Department of Orthopaedics and Traumatology, The University of Hong Kong, Hong Kong SAR，China

[3]Department of Biomedical Engineering, Southern University of Science and Technology, Shenzhen, Guangdong, China

[4] Faculty of Pharmaceutical Sciences, Shenzhen Institute of Advanced Technology, Chinese Academy of Sciences, Shenzhen, China

[#]These authors contributed equally to this work

*Corresponding author:

William Weijia Lu, PhD, University of Hong Kong, wwlu@hku.hk,

Fan Yang, PhD. Shenzhen Institute of Advanced Technology, fan.yang@siat.ac.cn;

Keywords: Parathyroid; subfornical organ; bone

Abstract

Parathyroid hormone (PTH) is one of the most important hormones responsible for bone turnover and calcium homeostasis. In mammals, PTH is secreted through the parathyroid glands, unlike in fishes, which are secreted through central nervous system. Studies indicated that a variety of peripheral nerve regulates serum PTH level, however, the mechanism underlying central neural regulation of PTH in mammals remains largely unknown. With an approach including neural-specific retrograde tracing, PTH-Biotin binding assay, and cFos staining, we identified the subfornical organ (SFO) and the paraventricular nucleus (PVN) as two important brain nuclei that responded to serum PTH and calcium changes. Using chemogenetics, we found that serum PTH was suppressed by stimulation of GABAergic neurons in SFO followed by a decrease in trabecular bone mass. Conversely, stimulation of glutamatergic neurons in SFO promoted serum PTH and bone mass. Moreover, we found that the majority of neurons expressing parathyroid hormone 1 receptor (PTH1R) were GABAergic neurons and the majority of neurons expressing parathyroid hormone 2 receptor (PTH2R) were glutamatergic neurons. The paraventricular nucleus (PVN) is downstream of the SFO, and chemogenetic activation of glutamatergic neurons in PVN induced an increase in serum PTH. In summary, our study demonstrates for the first time that distinct neuronal subtypes in the SFO are responsible for bidirectional regulation of serum PTH and bone metabolism, which is mediated through the PVN and the peripheral nervous system. These findings reveal important central neural nodes and will advance our understanding of the central neural regulation of PTH at the molecular, cellular and circuit level.

52 **Introduction**

53 Parathyroid hormone (PTH) is one of the most important hormones that modulate bone
54 remodeling and calcium homeostasis, which is conserved from zebrafish to humans[1,2].
55 In fish that do not have isolated parathyroid glands, PTH peptides are mainly expressed
56 in the lateral line, the neural tube and in the central nervous system[3-5]. In humans and
57 other mammals, PTH is mainly secreted from the parathyroid glands to maintain basal
58 serum calcium levels under different nutrient conditions. The secretion of PTH is finely
59 regulated by the humoral, hormonal stimulations, and the level of PTH is precisely
60 maintained based on the serum calcium concentration.

61

62 In the mammalian central nervous system (CNS), parathyroid hormone 2 receptors
63 (PTH2R) and TIP39 proteins form a unique neuropeptide–receptor system, in which
64 there is a wide distribution of axon terminals from neurons that support functions such
65 as nociceptive signaling and neuroendocrine regulation[6]. In the rat brain, PTH2-
66 receptor expression is observed in the cerebral cortex, stratum and hypothalamus,
67 including the arcuate nuclei and median eminence[7]. Recent work demonstrated that
68 ancient parathyroid hormone 4 (PTH4) appear to be a central neural regulator of bone
69 development and mineral homeostasis[5], and ablation of PTH4 neurons results in
70 abnormal bone mineralization and osteoblast differentiation in zebrafish[8]. These
71 findings support that PTH or PTH receptors might have played a continuous prominent
72 role in the brain-to-bone signaling pathway and in the maintenance of bone homeostasis
73 during vertebrate evolution. However, whether the adult mammalian central nervous
74 system has retained the capacity to detect PTH levels and direct the neural regulation
75 of PTH homeostasis is largely unknown.

76

77 In addition to the CNS, abundant levels of neural terminal expression have been
78 observed in parathyroid glands[9-14]. Administration of epinephrine or isoproterenol
79 infusion acutely induces PTH release, which is ablated by the β-adrenergic receptor 2
80 antagonist propranolol[15], and direct stimulation of parathyroid nerves upstream of the
81 parathyroid induces serum PTH elevation[16]. Clinical studies have also shown that
82 neuropsychiatric symptoms including anxiety, depression and cognitive impairments
83 are prevalent in patients with hyperparathyroidism, which, along with bone
84 abnormalities, are significantly improved after parathyroidectomy[17,18]. Based on this
85 evidence, we hypothesized that distinct brain nuclei and neuronal subtypes may sense
86 PTH levels and direct peripheral nerves to regulate PTH secretion in a top-down manner.
87 However, it is not clear what these important nodes in the central nervous system that
88 control PTH secretion in mammals are, or the underlying mechanisms.
89
90 In this study, we firstly identify the subfornical organ (SFO), a member of the
91 circumventricular organs (CVO), as an important brain nucleus modulating the
92 homeostasis of PTH. Chemogenetic activation of glutamatergic and GABAergic
93 neurons in SFO exerted responses in opposing directions in serum PTH and tibiae
94 trabecular bone mass. Neurons in the SFO express PTH receptors 1 and 2, the majority
95 of which are expressed in GABAergic and glutamatergic neurons, respectively.
96 Activation of glutamatergic nerves in paraventricular nucleus (PVN), which are
97 downstream of the SFO, led to elevated serum PTH and trabecular bone mass. In
98 addition, sympathetic and sensory nerves were identified within the parathyroid glands,
99 and ablation of these affected serum PTH levels and PTH response to calcium. Our
100 study not only demonstrates that the central nervous system is indispensable for the
101 regulation of peripheral PTH secretion and maintenance of bone-metabolism

homeostasis, but also for the first time revealed the underlying mechanism of central neural regulation of the PTH at molecular, cellular and circuit level.

Results

Parathyroid glands are connected to the central nervous system

Previous studies have demonstrated that parathyroid glands (PTG) receive sympathetic, parasympathetic, and sensory neural innervation, however, the central source of this innervation was not clear. To determine the brain nucleus that innervates the parathyroid gland (PTG), we injected the neural retrograde tracer pseudorabies virus (PRV-GFP) directly into the PTG (Fig. 1A-F). It could be observed the pseudorabies virus infects the central nervous system through the brain stem initiating from the intermediate reticular nucleus (IRt) and raphe magnus nucleus (RMg) (Fig. 1C-D). From the date of virus administration, it usually takes 7 days for the virus to infect from brainstem to midbrain and then to the hypothalamus and forebrain (Fig. 1E). The brain nuclei with the highest PRV expression markers on the 7th day of infection included: the median preoptic nucleus (MnPO), subfornical organ (SFO), suprachiasmatic nucleus (SCh), the nucleus of the vertical limb of the diagonal band (VDB), and Arcuate nucleus (Arc) (Fig. 1F, Supplementary Fig. 1). The MnPO and SFO and area postrema (AP) belongs to a group called the circumventricular organs (CVO), which are characterized by their extensive and highly permeable microvasculature and have no blood-brain-barrier[19].

We then performed a PTH-Biotin binding assay to determine whether peripheral administrated PTH can enter the central nervous system and bind directly to brain. Positive PTH-Biotin binding sites were assessed using immunofluorescence staining of biotin, and injection of saline and biotin was also performed as negative controls. The

127 brain nuclei detected with biotin binding includes the SFO, periventricular
128 hypothalamic nucleus (pv), SCh, periventricular hypothalamic nucleus (Pe), AP and the
129 nucleus tractus solitarius (NTS) (Fig. 1G, Supplementary Fig. 2). The majority of
130 identified nuclei were located surrounding the brain ventricles. Joborn et al reported
131 high-level expression of PTH in human cerebrospinal fluid, especially in
132 hyperparathyroidism patients[20]; our results support this by showing that peripheral PTH
133 can indeed enter the central nervous system and bind to specific brain nuclei.
134
135 To investigate the brain nuclei responsive to peripheral PTH, we injected human PTH
136 (1-34) or saline intravenously into C57 mice *i.p.* Neuronal activation was assessed
137 following cFos immunostaining, and cFos positive cells were quantified in different
138 brain nuclei. We found that neurons in a variety of brain nuclei, including the SFO,
139 paraventricular thalamic nucleus (PVN), anterior paraventricular thalamic nucleus
140 (PVA) and suprachiasmatic nucleus (SCh) were activated by serum PTH
141 (Supplementary Fig. 3), and the number of cFos positive cells in the SFO and PVN
142 significantly increased after PTH injection (Fig. 1H).
143
144 Using the three above-mentioned methodological approaches, we identified the SFO as
145 one prominent brain nucleus that is both physically and functionally connected to the
146 parathyroid gland. The SFO is an important area in the forebrain, a member of the
147 sensory circumventricular organs (sCVO)[19], which play an important role in the
148 regulation of water and sodium intake[21]. To further confirm the direct effects of PTH
149 on SFO neurons, we used patch clamp recordings to observe the direct neuronal
150 response to PTH. Application of PTH (10^{-6} M) led to significantly increased SFO
151 neuron resting potentials and firing rates (Fig. 1I). In summary, these results

152 demonstrate that the parathyroid glands receive synaptic connections from a variety of
153 brain nuclei, and that SFO neurons directly respond to peripherally administered PTH.
154

155 **Activation of SFO^{GAD} and SFO^{VGlut} neurons have different effects on the**
156 **regulation of PTH and bone remodeling**

157 Neurons in the SFO detect serum nutrients and osmotic pressure directly through leaky
158 blood vessels and regulate drinking and feeding behavior through downstream nuclei[22-
159 26]. To investigate whether neural activity of the SFO modulates serum PTH levels, we
160 activated SFO neurons directly and analyzed serum PTH changes (Fig. 2A). Because
161 calmodulin-dependent protein kinase II (CaMKII) was previously identified as a marker
162 of excitatory neurons in the SFO[22,27], we activated SFO^{CaMKII} neurons through
163 chemogenetic and optogenetic approach respectively. Chemogenetic modulation was
164 performed by transduction of AAV9-CaMKII-hM3Dq-mCherry into the SFO and
165 Clozapine-N-oxide (CNO) was used to activate SFO^{CaMKII} neurons. We found that acute
166 activation of SFO^{CaMKII} neurons induced 29.0% decrease of serum PTH level 30 mins
167 after CNO administration (Supplementary Fig. 4A). Optogenetic modulation was also
168 performed by transduction of AAV9-CaMKII-ChR2-mCherry into SFO and blue light
169 was used to activate the neurons. Optogenetic stimulation of SFO^{CaMKII} for 15 mins
170 induces 17.1% decrease of serum PTH level (Supplementary Fig. 4B), suggesting a
171 direct response of PTH secretion to SFO neural activities. To study the long-term effect
172 of SFO^{CaMKII} neuron stimulation on the PTH and bone structure, we performed CNO
173 administration every 48 hrs for 1 month. There was significantly lower serum PTH
174 (23.6% lower) in the hM3Dq group than in the control group following activation of
175 SFO^{CaMKII}, but no difference in serum calcium levels (Fig. 2A). After chronic
176 stimulation for 4 weeks, bone mineral density (BMD) of the tibiae trabecular bone was

177 19.6 % lower than the control group (Fig. 2A), accompanied by lower trabecular bone
178 volume fraction (BV/TV) and trabecular number (Tb.N) (Supplementary Fig. 4C).
179 However, the BMD of cortical bone was similar between groups (Fig. 2A). Both the
180 rapid and long-term effect of chemogenetic regulation on PTH level supported a direct
181 causal relationship between SFO activity and PTH regulation.
182
183 Previous studies have indicated that the SFO contains intermingled populations of
184 glutamatergic and GABAergic neurons, one which triggers and one which curbs thirst[22].
185 To explore whether glutamatergic and GABAergic neurons are involved in regulating
186 PTH, we investigated colocalization of CaMKII with gamma-aminobutyric acid
187 (GABA) and vesicular glutamate (VGlut). We found that 32.2% of AAV9-CaMKII-
188 mCherry-labeled neurons expressed GABA in the SFO, whereas 59.7% of CaMKII-
189 labeled neurons colocalize with VGlut (Fig. 2B). We then assessed colocalization of
190 cFos expression and VGlut2/glutamic acid decarboxylase (GAD, enzyme that catalyses
191 the conversion of glutamate to GABA)1&2 expression in SFO induced by peripheral
192 PTH (Fig. 2C). Of the SFO neurons activated following peripheral PTH application,
193 we found an intermingled mixture with 43% glutaminergic and 45% GABAergic
194 neurons (data not shown), suggesting that both type of neurons can be activated by PTH.
195
196 To further investigate the regulatory function of GABAergic and glutamatergic neurons
197 in the SFO, we performed chemical genetic stimulation using the AAV9-GAD67-cre
198 virus and the AAV9-DIO-hM3Dq system (Fig. 2D), and we found that specific
199 stimulation of SFO^{GAD} neurons induced a significant decrease of PTH (32.1%) and
200 tibiae trabecular BMD (20.7%), whereas serum calcium levels and cortical BMD were
201 not significantly different from controls (Fig. 2D, Supplementary Fig. 5A). Similarly,

202 we used VGlut2-Cre mice and the AAV9-DIO-hM3Dq system to stimulate SFO^{VGlut}
203 neurons, and chemogenetic stimulation resulted in a 45.3% increase of serum PTH and
204 29.1% increase in tibia trabecular BMD accompanied by a significant increase in
205 BV/TV, trabecular numbers and trabecular spaces (Fig. 2E, Supplementary Fig. 5B).
206 These results demonstrated that SFO^{GAD} and SFO^{VGlut} neurons both regulate serum
207 PTH levels and bone metabolism, however the effects of these two distinct neuronal
208 populations on the regulation of PTH and bone remodeling appear counter each other,
209 indicating that the CNS bi-directionally regulates PTH level through isolated pathways.
210

211 **PTH receptors expressed in SFO neurons regulate negative feedback of PTH**
212 **secretion**

213 Since peripheral PTH can directly bind and activate SFO neurons (Fig. 1E-F), we next
214 assessed PTH-receptor expression in the SFO and their function in the regulation of
215 serum PTH. In order to study the PTH1R/PTH2R expression in glutamatergic and
216 GABAergic neurons in the SFO, we used colocalization staining and found that PTH1R
217 and PTH2R were both expressed in SFO^{VGlut} and SFO^{GAD} neurons (Fig. 3A-C).
218 Quantification revealed that the majority of cells that expressed PTH1R were
219 GABAergic (81.0%) compared to glutamatergic neurons (53%) (Fig. 3C). Conversely,
220 the majority of PTH2R cells were glutamatergic (73.7%) compared to GABAergic
221 neurons (54.4%) (Fig. 3C).
222

223 Neurons expressing PTH2R are widely distributed in the central nervous system
224 including the locus coeruleus (LC), amygdala, and the periaqueductal gray (PAG), and
225 their functions are correlated with pain and nociceptive behaviors[28-30]. Expression of
226 PTH1R in the SFO was also demonstrated by *in situ* hybridization in the Allen Brain

227 Atlas (Pth1r-RP_110421_01_D07-coronal), however PTH1R function in the brain has
228 not been studied in detail. To investigate the function of the PTH1R and PTH2R in
229 maintaining PTH homeostasis, we down-regulated PTH1R and PTH2R expression in
230 the SFO using LV-PTH1R-Cas9 or LV-PTH2R-Cas9 respectively (Fig. 3D). The
231 knockdown efficiency within SFO was assessed through immunofluorescence staining
232 against PTH1R or PTH2R respectively (Supplementary Fig. 6A-B). The percentage of
233 $PTH2R^+$ cells has decreased from 48.3% in control group to 14.5% in $PTH2R^-$ group,
234 while the $PTH1R^+$ cells has decreased from 53.8% in control group to 23.1% in $PTH1R^-$
235 group (Supplementary Fig. 6C). Serum basal PTH was determined after the knockdown,
236 we found that PTH in PTH1R knockdown group was 20.4% lower than the control
237 group, while PTH level of the PTH2R knockdown group was comparable with the
238 control group (Fig. 3D-E). The serum total calcium remains unaffected in all three
239 groups (Fig. 3E). The effects of knockdown of PTH2R/PTH1R in SFO on bone were
240 also studied by MicroCT analysis. Neither BMD of tibial trabecular bone and femoral
241 cortical bone was affected, however Tb.N increased and Tb.Sp decreased after the
242 knockdown of PTH1R compared to the control group (Fig. 3H-K, Supplementary Fig.
243 6D).
244
245 To further investigate the effects of the parathyroid hormone receptors on maintaining
246 PTH homeostasis, animal was administrated with 3 μM of $CaCl_2$ *i.p.* to induce
247 hypercalcemia and the serum PTH and total calcium was assessed before and 5, 15, 30
248 min after the stimulation (Fig. 3F-G). In response to acute calcium increase, the serum
249 PTH of control group show consistent decrease from the 15th min (A15) to 30th min
250 after injection (A30). The serum calcium level of the control group increased by A5 and
251 decreased rapidly afterwards and returned to normal by the time A30. However, for the

252 SFO^{PTH1R-} and SFO^{PTH2R-} groups, both PTH level increased after calcium stimulation
253 and reached peak by A15 and began to decrease indicating a later latency of PTH
254 regulation response. The serum calcium level of the SFO^{PTH2R-} group increase and
255 reversed by the same time of control group with larger amplitude than the control group,
256 however, the calcium level of SFO^{PTH1R-} group failed to return to normal by A30 (Fig.
257 3G). These results indicate that knockdown of PTH receptors in SFO not only affected
258 PTH basal secretion, but also affect the kinetics of PTH in response to hypercalcemia
259 stimulation.
260
261 We also performed the fluid consumption tests in the SFO^{PTH1R} and SFO^{PTH2R}
262 knockdown mice since SFO is important organ for water-salt balance. It was found
263 knockdown of PTH1R in SFO induced a decreased water consumption compared to
264 control group, while PTH2R knock down in SFO did not show an effect
265 (Supplementary Fig. 6E).
266
267 Previous studies of the function of PTH2R in brain were mainly performed through
268 universal knockout experiments[30,31]. To further gain more insight into the function of
269 PTH2R neurons in SFO, we constructed a PTH2R-creER^{T2} transgenic mouse strain
270 (Supplementary Fig. 7-9). The successful construction of a PTH2R-creER^{T2} mice was
271 validated though cross breading of PTH2R-creER^{T2} mice with Ai14 mice resulting in
272 tdTomato protein expression in Cre-recombinase expressing cells.
273 Immunofluorescence staining of PTH2R was performed in PTH2R-creER^{T2} X Ai14
274 mice brain, and positive signals was observed in SFO, Arc, PVN, MPOL and a variety
275 of brain nuclei previously reported with high PTH2R expression[32] (Supplementary Fig.
276 7A, Supplementary Fig. 9). Colocalization staining with NeuN also demonstrated that

277 the majority of PTH2R^{+} cells in the SFO are neurons (Supplementary Fig. 7B). Then
278 we investigated the function of PTH2R expressing neurons in SFO, chemogenetic
279 activation of PTH2R neurons resulted in a 20.9% increase in serum PTH and no
280 changes in serum calcium (Supplementary Fig.7E), which is consistent with the effects
281 of activation of SFO^{VGlut} neurons. However, trabecular and cortical BMD was not
282 affected (Supplementary Fig. 7F). In the open field study, mice in hM3Dq group spend
283 less time in central areas while central entries, and total distance was not affected
284 (Supplementary Fig. 8A). There was also no difference between groups in the total
285 immobility time in tail suspension test (Supplementary Fig. 8B). Chemogenetic
286 activation of SFO^{PTH2R} also led to a higher intake of water compared to the control
287 group (Supplementary Fig. 8C). Taken together, our data demonstrated that PTHR
288 expressing neurons in SFO are essential in both sensing PTH/calcium levels and
289 regulating PTH secretion; PTH1R and PTH2R play different roles in regulating the
290 basal PTH secretion, PTH homeostasis in response to exogenous CaCl2 stimulations
291 and bone remodeling.
292
293 **PVN regulation of PTH**
294 Next, we investigated the downstream effectors of SFO neurons. We know that
295 SFO^{CaMKII} neurons project to a variety of brain nuclei including the MnPO,
296 paraventricular nucleus (PVN), Vascular organ of lamina terminalis (OVLT) and bed
297 nucleus of the stria terminalis (BNST)[21] (Supplementary Fig. 10). Of these brain nuclei,
298 the PVN is reported as crucial in the regulation of both neuroendocrine homeostasis
299 and sympathetic activity, then we investigated whether PVN neurons are involved in
300 the regulation of PTH and bone metabolism.
301

302 Unlike the SFO, which consists of both GABAergic and glutamatergic neurons, we
303 found that the majority of PVN neurons responding to peripheral PTH stimulation
304 (cFos-positive) were colocalized with VGlut2 and not GAD1&2 (Fig. 4A).
305 Immunofluorescence showed that CaMKII and VGlut2 are both abundantly expressed
306 in the PVN. Quantification revealed that VGlut2/CaMKII double-positive cells
307 accounted for 62.6% of VGlut2-positive neurons, and 67.7% of CaMKII-positive
308 neurons (Fig. 4B).
309
310 Next, we investigated the regulatory functions of PVN^{CaMKII} and PVN^{VGlut} neurons.
311 Chemogenetic activation of PVN^{CaMKII} neurons induces 63.0% increase in serum PTH
312 level 30 min after CNO administration (Supplementary Fig. 11A-B). After chronic
313 chemogenetic activation of PVN^{CaMKII} neurons for 1 month, the serum PTH level in the
314 hM3Dq group became 62.2% higher than the mCherry group (Fig. 4C). There was no
315 difference in the serum total calcium, BMD of tibial trabecular or femoral cortical bone
316 or trabecular microstructures between groups (Fig. 4C,4E, Supplementary Fig. 11C).
317 Interestingly, we activated PVN^{VGlut} neurons after transduction hM3Dq through
318 injection of the AAV9-DIO-hM3Dq-mCherry into the PVN of VGlut2-Cre mice (Fig.
319 4D) and found that chronic activation of PVN^{VGlut} neurons led to significantly higher
320 serum PTH than the control group (55.0%), and a higher trabecular BMD in mice tibiae
321 (35.4%) (Fig. 4D, Fig. 4F). Both percent bone volume and trabecular separation were
322 significantly changed in the experimental group (Supplementary Fig. 11F). These data
323 suggest that the activation of glutamatergic neurons in PVN efficiently up-regulate PTH
324 levels and bone remodeling.
325
326 **GABAergic neurons in the SFO send neuronal projections to the PVN and**

327 **regulate bone remodeling**

328 Direct SFO^{CaMKII} projection to the PVN has been observed by Zimmerman, et al. [25].
329 However, it is not known whether the PVN receives an SFO^{GAD} projection. We studied
330 SFO^{GAD} neuronal projections using a combined injection of AAV9-DIO-mCherry and
331 AAV9-GAD67-Cre viruses into the SFO of C57 mice. In addition to the previously
332 described SFO^{VGAT}→MnPO and SFO^{VGAT}→OVLT neuronal projection (VGAT,
333 vesicular GABA transporter, that loads GABA from the neuronal cytoplasm into
334 synaptic vesicles)[22,26], we found that the PVN also receives dense innervation from
335 SFO^{GAD} neurons (Fig. 5A). To confirm that the PVN^{VGlut} neurons specifically receive
336 synaptic connections from SFO^{GAD} neurons, we performed retrograde tracing by
337 injecting AAV9-DIO-TVA-RVG and RV-ΔG-mCherry into the PVN of VGlut2-Cre
338 mice (Fig. 5B). Efficient transfection of AAV helper and RV in PVN glutamatergic
339 neurons was indicated by mCherry signals in the PVN. In the SFO, RV positive
340 mCherry signals, which were colocalized with GABA and CaMKII, indicated
341 retrograde monosynaptic connection with PVN^{VGlut} neurons (Fig. 5B).

342

343 To explore regulatory function in SFO^{GAD} -PVN circuit, we injected AAV9-GAD67-
344 Cre virus into the SFO and AAV2retro-DIO-hM3Dq-mCherry virus into the PVN of
345 C57 mice. Specific chemogenetic activation of the neural projections from SFO^{GAD} -
346 PVN circuit induced 20.8% decrease of serum PTH level and 18.4% decrease of serum
347 calcium level within the hM3Dq group (Fig. 5C). The tibial trabecular BMD was also
348 decreased by 5% while femoral cortical BMD was not affected (Fig 5C-D). Trabecular
349 BV/TV and Tb.N were also decreased in hM3Dq group (Supplementary Fig. 12A). In
350 the behavior test, the water and salt consumption were not affected during the activation
351 of the SFO^{GAD}→PVN circuit (Supplementary Fig.14B). These results reveal a novel

352 SFO^{GAD}-PVN circuit which specifically regulates serum PTH, total calcium and
353 trabecular bone metabolism.
354
355 **Ablation of sympathetic nerves affect serum PTH level**
356 Innervation of parathyroid glands has been reported in previously studies. In our study,
357 we observed both the sympathetic nerves (TH^+) and sensory nerves which were labeled
358 with calcitonin gene related protein ($CGRP^+$) in the parathyroid gland (Fig. 6A-B).
359 Double staining revealed sympathetic nerves in mice parathyroid glands, which form a
360 net-like structure that surrounds the blood vessels ($CD31^+$); the sympathetic nerves
361 form clusters with blood vessels rather than an even distribution in the parathyroid
362 glands (Fig. 6B). On the other hand, most CGRP nerves were observed between
363 parathyroid-gland substructures as single neural fibers (Fig. 6B).
364
365 Physical connectivity between the parathyroid glands and the nervous system was also
366 investigated using neuronal-specific retrograde tracing from the parathyroid glands. We
367 injected CTB-Alexa Fluor 488 into one side of the rat parathyroid glands and then after
368 sacrifice, both side of the sympathetic superior cervical ganglia (SCG) and inferior
369 vagal ganglia (Vagus) were isolated to study innervation. CTB signals were observed
370 in both sides of the SCG and Vagus (Supplementary Fig. 13). These results are
371 consistent with the findings of both sympathetic nerves and CGRP nerves in parathyroid
372 glands.
373
374 Next, we performed RV tracing using PTH-Cre mice to assess whether there is direct
375 synaptic connectivity between parathyroid chief cells and the peripheral nervous system.
376 The signals of both RV and helpers were observed in parathyroid glands in PTH-Cre

377 mice, indicating that the AAV helper and RV had infected parathyroid chief cells (Fig.
378 6C-D). One week after virus infusions, positive RV signals were observed in the SCG
379 and Vagus following counterstaining of tyrosine hydroxylase (TH) in the SCG, choline
380 acetyltransferase (ChAT) and calcitonin gene-related protein (CGRP) in the Vagus (Fig
381 6E-G). These results indicate that the SCG and Vagus may be directly connected to the
382 parathyroid chief cells by direct, monosynaptic connections.
383
384 The function of peripheral sympathetic nerves in the regulation of PTH was
385 investigated further through ablation of peripheral sympathetic neural terminals by 6-
386 OH-Dopamine. The sympathetic nerve terminals were ablated universally in mice
387 through *i.p.* administration in mice (Fig. 6H-J) and locally within the parathyroid glands
388 in rats (Fig. 6K-M). Universal ablation of sympathetic neural terminals in mice induced
389 a decrease of basic serum PTH (Fig. 6J), and the serum PTH level was also not
390 responding to the hypercalcemia stimulation (Fig. 6J). After the ablation of the
391 sympathetic nerve terminals in PTG of rats, basal PTH level were not affected, however
392 the serum PTH was not responding to the hypercalcemia stimulation in the 6-OHDa
393 group compared with the control group (Fig. 6M). Taken together, these data
394 consistently demonstrate that the sympathetic and sensory nervous system are both
395 tightly integrated with the parathyroid glands, and that the ablation of peripheral
396 sympathetic nerve significantly impacts PTH response to hypercalcemia stimulation.
397
398 **Discussion**
399 Modulation of serum calcium levels and bone remodeling relies upon serum PTH, the
400 most important hormone in this regard, levels of which are maintained through humoral,
401 hormonal and neural regulation[33]. However, until now the effects of central neural

402 regulation of serum PTH and underlying mechanisms were largely unknown. Using
403 neural circuit tracing and chemogenetic techniques in addition to analysis of PTH and
404 bone metabolism, we for the first time, systemically studied the structural and
405 functional connection between the parathyroid and specific types of neurons in the
406 central nervous system. This resulted in the identification of the components of a
407 specific central neural circuit that modulates PTH and in the revelation of the
408 underlying mechanism of central neural regulation of PTH levels and bone metabolism
409 (Supplementary Fig. 14).
410

411 **Central nervous system (CNS), PTH and bone metabolism**

412 The close relationship of PTH to the CNS has been observed for decades. The earliest
413 studies suggesting PTH function within the CNS stem from a series of findings
414 beginning with the identification of PTH-like immunoreactive protein in the brains of
415 different species, particularly in bony fish. In mammals, the embryonic origin of
416 parathyroid gland is derived from the 3rd and 4th brachial pouch, which closely
417 neighbors the neural crest (NC) mesenchyme[34,35]. An evolutionary model has also been
418 proposed, in which, during the evolutionary period where aquatic vertebrates
419 transitioned to a terrestrial environment, the parathyroid gland gradually migrated from
420 the CNS to the periphery to enhance calcium regulatory capacity during times of
421 unstable calcium dietary supplementation[2]. However, the question of whether the CNS
422 still reserves calcium and PTH regulation functionality in adult mammals has never
423 been asked. In this study, we provide the first demonstration that chemogenetic
424 activation of SFO^{GAD}, SFO^{VGlut}, PVN^{CaMKII} and PVN^{VGlut} neurons are able to directly
425 modulate serum PTH levels and the bone metabolism in the absence of any other
426 experimental manipulation. Conversely, knocking down the expression of PTH1R and

427 PTH2R in the SFO, or ablation of the sympathetic nerves in the PTG, led to a significant
428 blockade of serum PTH and calcium responses to exogenous calcium stimulation. This
429 evidence demonstrates the necessity of the central and peripheral nervous systems in
430 both regulating PTH basal secretion and maintaining PTH homeostasis through
431 feedback loops.
432
433 Parathyroid hormone is an important hormone in the bone remodeling process, where
434 it initiates bone resorption followed by bone formation[1]. Ablation of PTH4 neurons
435 result in abnormal bone mineralization and significantly affects osteoblast
436 differentiation[8], suggesting that PTH might be an important regulator of the central
437 neural control of bone remodeling. In our study, we found that changes in bone mass
438 were typically in the same direction as PTH changes; that is, decreased PTH was
439 followed by decreased tibiae trabecular BMD and increased PTH was followed by
440 increased tibiae trabecular BMD. Previous studies have indicated that intermittent
441 administration (daily) of PTH induces an anabolic effect in bone, which is contrary to
442 the effects of continuous administration[1]. In our study, chemogenetic activation of brain
443 neurons was performed with transduction of hM3Dq in the brain and administration of
444 CNO (*i.p.*) every 48 hours. Based on a pharmacokinetic study of CNO[36], serum PTH
445 changes induced by chemogenetic stimulation of mice reached peak levels every 48
446 hours, which may explain the anabolic effects of PTH on bone.
447
448 **SFO neurons are important in both the detection and regulation of PTH level**
449 Both the short-term and long-term effect of chemogenetic regulation on PTH level
450 supported the direct causal relationship between SFO activity and PTH regulation. As
451 a member of the CVO, the SFO directly detects circulating molecular signals in serum.

452 We found PTH1R and PTH2R expression in SFO neurons, reaffirming this finding
453 reported in the Allen Brain Atlas database. The binding efficiency of PTH1R to PTH is
454 different from that of PTH2R. The EC50 of PTH1R to PTH (1-34) is around 1-2 nM,
455 whereas the EC50 of PTH2R to PTH (1-34) is around 70 nM[37]. Therefore, serum PTH
456 in healthy individuals (65-150 pg/mL) would likely predominantly activate only
457 PTH1R in the SFO. In our study, we found that PTH1R expression was predominant in
458 SFO^{GAD} neurons and activation of SFO^{GAD} neurons induced a decrease in serum PTH.
459 It is thus expected that, under physiological conditions, the CNS can modulate serum
460 PTH in a negative feedback pathway mainly through SFO^{GAD} neurons.
461
462 On the other hand, under severe pathological conditions such as hyperparathyroidism
463 (HPT), serum PTH levels are around 10-100 times higher than physiological levels and
464 SFO^{VGlut} neurons, which mainly expressed PTH2R, would be activated to induce a
465 consistent increase of serum PTH. Our study indeed found that chemogenetic activation
466 of the SFO^{VGlut} neurons did induce a significant elevation of PTH levels and increased
467 bone density, which is a reverse of the regulatory effects of SFO^{GAD} neurons. Our
468 findings may thus explain why serum PTH becomes uncontrollable in some patients of
469 late-stage HPT and leaves them with no other treatment except parathyroidectomy
470 surgery.
471
472 In addition, it is consistently reported that HPT patients develop psychiatric symptoms
473 including anxiety, depression and cognitive disorder[38]. Moreover, if these symptoms
474 develop in primary or secondary HPT diseases, they improve following
475 parathyroidectomy surgery[17,39-41]. The function of PTH2R and the agonist TIP39
476 mediate nociception, including neuropathic and inflammatory pain[29]; genetic

477 knockdown of PTH2R in the medial amygdala and disruption of PTH2R projections to
478 the bed nucleus of the stria terminalis (BNST) influence fear- and anxiety-like behavior
479 [30,42]. However, there are no gain of function studies for PTH2R reported in the literature.
480 In our study, we firstly found that knockdown of *pth2r* in the SFO did not induce
481 behavioral changes. However, chemogenetic activation of SFO^{PTH2R} neurons in
482 PTH2R-creER^{T2} mice led to less time in the center during OFT tests, which is used as
483 an index of anxiety, even although immobility time during TST was not affected. These
484 data indicate that PTH2R neurons in the SFO regulate anxiety-like behaviors in mice,
485 in addition to regulating PTH level and the bone remodeling process.
486
487 **The PVN, sympathetic nerves and the PTH**
488 Of the nuclei downstream of the SFO, we chose the PVN as the target to study its
489 function in the regulation of PTH. In addition to the fact that PVN receives polysynaptic
490 connections from the PTG and is responsive to peripherally administrated PTH and
491 calcium, the PVN receives a direct monosynaptic neural projection from SFO
492 GABAergic neurons as revealed by our RV tracing study. The PVN is well known as
493 crucial member of the neural-humoral hypothalamic-pituitary-thyroid (HPT) axis and
494 the hypothalamic-pituitary-adrenal (HPA) axis[43]. In addition, PVN^{VGlut} neurons also
495 directly project to the nucleus tractus solitarius (NTS), which affects sympathetic
496 nerves through a neural sympathetic connection[44]; activation of PVN^{VGlut} neurons
497 increase the activity of the sympathetic nervous system[45].
498
499 By directly activating PVN neurons, we primarily found that activation of PVN neurons
500 results in elevated serum PTH levels, and found different regulatory effects following
501 activation of PVN^{CaMKII} or PVN^{VGlut} neurons, despite overlap of these neurons.

502 Activation of both PVN^{CaMKII} and PVN^{VGlut} induced an increase in serum PTH, however,
503 trabecular BMD was not affected following PVN^{CaMKII} activation yet increased
504 following PVN^{VGlut} activation. These findings suggest that PVN^{VGlut} neurons are more
505 likely to regulate both PTH levels and bone metabolism compared to PVN^{CaMKII}
506 neurons, since PVN^{VGlut} neurons directly receive a monosynaptic projection from
507 SFO^{GAD} neurons. Previous research has indicated that noradrenergic neurons in the
508 PVN suppress stress-induced bone loss[46], whereas our study shows that PVN^{VGlut}
509 neurons exerted more of an effect on bone metabolism through the regulation of PTH.
510 The inhibitory effects on trabecular bone BMD following specific activation of the
511 GABAergic neural projection from the SFO to the PVN further confirmed that PVN
512 can relay upstream signals from the SFO to regulate bone metabolism (Figure 5).
513 However, neural activation of SFO and PVN may also lead to systematic effects on
514 other organs resulting in indirectly influence on PTH and bone, which requires further
515 study in future.
516
517 Previous work has indicated that serum PTH increased tenfold during electric
518 stimulation of the cerebral sympathetic trunk (CST)[16]. Consistent with this, we found
519 that ablation of peripheral sympathetic nerves in mice induced a significant decrease of
520 serum PTH. This finding is also consistent with an earlier study in which direct infusion
521 of epinephrine induced 127 to 255% increase of PTH in cows[15]. From our
522 immunofluorescence study, we found that TH nerve terminals were tightly surrounded
523 by the capillaries within the PTG, indicating that serum PTH may be regulated
524 sympathetically via capillary vasodilation and contraction. The neural tracing
525 experiments and ablation study further confirmed that sympathetic innervation is
526 necessary for relaying the central signals to regulate PTH homeostasis.

527

528 In summary, our contributions are in three parts. Firstly, we identified the SFO and PVN
529 as important nodes that regulate serum PTH levels and bone metabolism. Secondly, for
530 the first time, we revealed a population of GABAergic neurons in the SFO, which not
531 only detect PTH levels via PTH receptors, but also directly regulates PTH levels.
532 Thirdly, we found that the PVN and peripheral sympathetic system were downstream
533 of the SFO in this circuit and play important roles in the regulation of PTH homeostasis
534 and bone metabolism. Therefore, not only did we identify the underlying mechanism
535 of central neural regulation of serum PTH, but also provide evidence of the intricate
536 process by which the CNS detects peripheral PTH and the responses to changes in
537 serum PTH under physiological or pathological conditions.

538

539 **Methods**

540 **Animals**

541 C57/6J mice and SD rats (Beijing Vital River Laboratory Animal Technology Co) raised
542 at the Shenzhen Institute of Advanced Technology, Chinese Academy of Science were
543 used. VGlut2-ires-cre mice (Jackson Laboratory, 016863), PTH-cre mice (Jackson
544 Laboratory, 005989), Ai14 mice (Jackson Laboratory, 007908) were also used. PTH2R-
545 CreER^{T2} mice were established and provided by GermPharmatech Co., Ltd. Only male
546 mice/rats of 6-8 weeks-old were used in this study. All animals were housed under a
547 Specific Pathogen Free (SPF) barrier environment according to the standard of
548 GB14925-2010 Laboratory Animals Requirement of Housing and Facilities within a
549 temperature-controlled room (20-26°C) with a 12-hour light/dark cycle (07:00 lights
550 on, 19:00 lights off). Animals had free access to chow and water. All studies and
551 experimental procedures were approved by the Institutional Animal Care and Use

552 Committee (IACUC) of the Shenzhen Institute of Advanced Technology, Chinese
553 Academy of Science.
554
555 PTH2R- CreER^{T2} mice were generated based on C57/6J mice using the CRISPR-Cas9
556 technique by inserting a strand of cre recombinase with an estradiol receptor (ERT2)
557 after the PTH2r promoter. Tamoxifen (75 mg/kg, i.p.) was administrated to the animal
558 5 days before experiments to initiate cre recombinase gene expression.
559
560 **Retrograde neural tracing from parathyroid glands**
561 Neural specific retrograde tracing was conducted with chloral toxin B (CTB- Alexa
562 Fluor 488, 10 mg/mL, Molecular Probes®), modulated pseudorabies virus vector (PRV),
563 modulated rabies virus vector (RV) and its adeno-associated virus (AAV) helper. Non-
564 trans-synaptic retrograde tracing was conducted by CTB, which is absorbed by the
565 neural terminals and can be transported to the neuronal soma. Monosynaptic retrograde
566 tracing was performed with sequential use of AAV helper (DIO-EGFP-TVA-RVG) and
567 modulated RV (RV-EnvA-ΔG-dsRed). The AAV helper was used for Cre-dependent
568 expression of TVA, which directs the infection of RV and G proteins that reinstate the
569 trans-synaptic infection. Poly-synaptic retrograde tracing was employed by
570 pseudorabies virus (PRV-GFP), which infects the neural terminals of the injection site
571 and is delivered to the soma and transfects to the next neuron through synaptic
572 connection.
573
574 Helper AAV, RV and PRV (BrainVTA, Wuhan, China) were used with titers of 1.3E+12
575 PFU/mL, 5.0E+08 PFU/mL and 2.0E+09 PFU/mL, respectively. The retrograde tracers
576 were injected into the parathyroid glands of mice and rats using a Hamilton®

577 microsyringe under anaesthesia (*i.p.* 100mg/kg sodium pentobarbital). The precise
578 injection into mice PTG was performed through microscopic surgery and exclusion of
579 animals were carried out for the off-target injections.
580
581 **Virus injection and chemogenetic regulation of neurons**
582 Adult mice of 6-8 weeks were anaesthetized (*i.p.* 100mg/kg sodium pentobarbital) and
583 mounted on a stereotaxic frame (RWD Life Science, Shenzhen, China). Virus
584 suspension (AAV9-CaMKII-mCherry, AAV9-CaMKII-hM3Dq-mCherry, AAV9-
585 CaMKII-ChR2-mCherry, AAV9-DIO-mCherry, AAV9-DIO-hM3Dq-mCherry, AAV9-
586 GAD67-cre, AAV2retro-DIO-hM3Dq-mCherry, AAV2retro-DIO-EYFP, LV-PTH1R-
587 Cas9, LV-PTH2R-Cas9, LV-empty; 1.5-2.5E+12 PFU/mL) were loaded into a 5μl-
588 Hamilton® syringe with 33-g needle, and 150 nL was injected with a speed of 100
589 nL/min by the targeting locations (SFO: -0.58, 0, -2.5; PVN: -0.8, ±0.5, -4.5) based on
590 a stereotaxic atlas[47]. The surgical procedure was based on Lowery and Majewska[48].
591 After surgery, animals were allowed to recover for at least 1 week before experiments.
592 In chemogenetic studies, CNO (*i.p.* 1 mg/kg, MCE, 34233-69-7) was injected 3 weeks
593 after virus expression, every 48 hours for 4 weeks prior to serum and bone collection
594 and analysis. The AAV9 virus were all prepared in our lab, and the LV-PTH1R-Cas9,
595 LV-PTH2R-Cas9 and LV-empty were accessed from BrainVTA, Wuhan, China. The
596 precise injection into mice brain was performed and exclusion of animals were carried
597 out for the off-target injections.
598
599 **Optogenetic stimulation of CaMKII neurons in SFO**
600 C57 mice were injected with AAV9-CaMKII-ChR2-mCherry or AAV9-CaMKII-
601 mCherry into the SFO through stereotaxic injection. Three weeks after virus injection,

602 an optical fiber (200 μm diameter) was implanted 0.2 mm above with SFO with an
603 cannula fixed onto the skull. Optogenetic stimulation was performed 1 week after optic
604 fiber implantation. The light stimulation was performed with 450 nm blue light and
605 stimulated under 0.5-1 mW/cm^2, 20 Hz for 15 min.
606
607 **PTH and calcium neural activation experiments and PTH binding assay**
608 $CaCl_2$ (12 mM, Sigma, C5670), hPTH (1-34) (20 μg/mL, MCE, 52232-67-4), EDTA-
609 Na_2 (12 mM, Sigma, E9884), hPTH (1-34)-Lys (Biotin) (20 μg/mL, AnaSpec, AS-
610 23647) and Biotin (1 μg/mL,Sigma, B4501) were injected intravenously into C57 mice.
611 Animals were returned to their home cage and transcardially perfused for tissue
612 collection after 90-120 mins.
613
614 **Immunofluorescence staining and *in situ* hybridization**
615 Animals were anaesthetized with pentobarbital (100 mg/kg) and perfused intracardially
616 with PBS followed with 4% PFA. Tissue was collected and fixed in 4% PFA at 4 °C for
617 48 hours, and then dehydrated with 30% sucrose solution for 72 hours. Coronal sections
618 of brain (35 μm) and parathyroid glands (PTG, 15 μm) were cut using a Cryostat
619 microtome (Leica, CM1950) at -20 °C. The sections were washed twice with PBS and
620 blocked with blocking solutions (0.3% Tween20 in PBS with 5% goat normal serum or
621 5% bovine serum albumin) for 1 hour at room temperature, and then incubated
622 overnight at 4 °C with appropriate primary antibodies diluted in 0.03% PBST. The
623 primary antibodies used were: goat anti-Biotin (Sigma, F6762, 1:80), rabbit anti-
624 calcium sensing receptor (abcam, ab62214, 1:500), mouse anti-CaMKII (abcam,
625 ab22609, 1:500), goat anti-CD31 (R&D, AF3628, 1:20), rabbit anti-cFos (Cell
626 signaling, #2250, 1:200), mouse anti-CGRP (abcam, 81887, 1:500), rabbit anti-ChAT

627 (abcam, ab6168, 1:500), mouse anti cre-recombinase (Millipore, mab3120, 1:500),
628 rabbit anti-GABA (Sigma, ab2052, 1:500), chicken anti-GFP (abcam, ab13970, 1:1000),
629 rabbit anti-PTH (LSBio, LS-C191152, 1:500), rabbit anti-PTH1R (abcam, ab176393,
630 1:200), rabbit anti-PTH2R (abcam, ab188760, 1:200), mouse anti-TH (Sigma, T1299,
631 1:500), and chicken anti-NeuN (Millipore, ABN91, 1:500). Primary antibodies were
632 washed three times with 0.1% PBST, and then replaced with appropriate secondary
633 antibodies for 1 hour at room temperature and washed three times with 0.1% PBST.
634 The secondary antibodies used were: Goat anti rabbit Alexa Fluor 488/594 (Jackson
635 laboratory, 111-547-003/111-587-003, 1:200), Goat anti mouse Alexa Fluor 488/594
636 (Jackson laboratory, 115-547-003/115-587-003, 1:200), Anti-Goat IgG-FITC (Sigma,
637 F7367, 1:400), Donkey anti rabbit Alexa Fluor 647 (abcam, ab150075, 1:1000), and
638 Donkey anti goat Alexa Fluor 647 (abcam, ab150131, 1:1000). Sections were then
639 incubated with 0.5 μg/ml 4′,6-diamidino-2-phenylindole, dihydrochloride (DAPI;
640 ThermoFisher, D1306) for 1 min and Fluoromount-G (Southern Biotech, 0100-01).
641
642 *In situ* hybridization was performed to localize GABAergic and glutamatergic neurons
643 with *Vglut2*, *Gad1* and *Gad2* probes. The procedure of *in situ* hybridization followed
644 the procedure described by Kondoh et al.[49]. Quantification of cell numbers labeled with
645 different markers within different brain nuclei were calculated using 3 different slices
646 from 3-4 different animals based on DAPI expression. The average of the three slices
647 were taken and shown in graphs.
648
649 **Biochemical analysis**
650 Mouse and rat serum PTH levels were assessed with mouse and rat PTH ELISA kits
651 (LSBio, LS-5549/LS-5548). Total serum calcium levels were obtained using a

652 colorimetric assay (Sigma, MAK022). The results were read by a Nano Quant plate
653 reader (Tecan, Infinite 200Pro).
654
655 **Behavioral tests**
656 Anxiety levels were assessed by an open-field test (OFT). In the OFT, mice were placed
657 in a corner of a square field of 80 × 80 cm, with walls of 80 cm and sufficient
658 illumination. The movement of animals from the entrance of the field/maze was
659 recorded in an isolated room without interruption. The recording time for the OFT was
660 600 s. The time that each animal spent in different areas was assessed by analyzing
661 software (Anymaze) to evaluate anxiety levels. Tail suspension tests (TST) were
662 performed using a tail suspension cage (Bioseb, US). Mice were suspended by their tail
663 with tape on the force transducer and the recording time was 360 s. The time spent
664 immobile was analyzed using Anymaze within the Bioseb's suspension cage.
665
666 Fluid consumption tests were performed in cages with two bottles. Animals were single
667 housed to acclimatize to two bottles of water for 3 days and then completely water
668 restricted for 12 hours before the test. Two bottles of water and 300 mM NaCl solution
669 were provided to the animals during the test. Bottles were weighed every 2 hours within
670 the first 6 hours during which the animals were free to access the fluids. The position
671 of the bottles was changed after the first 1 hour to avoid position preference.
672
673 **Calcium tolerance test**
674 Animal blood samples were collected before and after administration of $CaCl_2$ (*i.p.* 3
675 μM for mice, 30 μM for rats) and serum PTH and calcium levels were assessed before,
676 5 min, 15 min and 30 min after administration. Blood was collected from the retro-

677 orbital sinus of mice and from the jugular vein from rats under anesthesia with
678 isoflurane.
679
680 **Micro-CT scanning and analysis**
681 Mice femur and tibiae were collected and immersed in 4% paraformaldehyde before
682 micro-CT scanning (SkyScan, model 1076). Scanning was performed using the
683 following settings: isotropic voxel 11.53 μm, voltage 48 kV, current 179 μA, and
684 exposure time of 1800 ms. Three-dimensional (3D) reconstruction was conducted using
685 SkyScan NRecon software (version 1.6.8.0, SkyScan) with a voxel size of 8.66 μm.
686 Datasets were reoriented using DataViewer (version 1.4.4.0, SkyScan), while the
687 calculation of morphological parameters was carried out with the CTAn software
688 (version 1.13.2.1, SkyScan). The 3D reconstructed models were displayed by CTVol
689 software (version 2.2.3.0, SkyScan).
690
691 Trabecular bone was selected 0.1-0.9 mm distal to the proximal tibia growth plate. The
692 region of interest (ROI) was selected from 2D images slice-by-slice by hand to exclude
693 the cortical area and then binarization of the images with a global thresholding of gray
694 level (70-255) as mineralized tissue, according to the tuning 3D reconstruction of the
695 mineralized tissue. A Gaussian filter (radius=1) was used for 3D reconstruction.
696 Quantitative analysis involved all bone areas within the ROI of the 3D images.
697 Morphometric parameters included total volume (TV, m^3), bone volume (BV, m^3), bone
698 fraction (BV/TV, m^3), trabecular thickness (Tb. Th, 1/mm), trabecular number (Tb. N,
699 1/mm), and trabecular separation (Tb. SP, mm). In addition, the bone mineral density
700 (BMD, g/cm^3) of the whole trabecular bone was calibrated using the attenuation
701 coefficient of two hydroxyapatite phantoms with defined mineral densities of 0.25 and

702 0.75 g/cm^3.

703

704 Cortical bone was selected 6.5-7.2 mm proximal to the distal femur growth plate. The
705 region of interest (ROI) was selected from 2D images with a threshold (85-255) as
706 mineralized tissue. A Gaussian filter (radius=1) was used for 3D reconstruction.
707 Quantitative analysis involved all bone areas within the ROI of the 3D images.
708 Morphometric parameters included BV and BMD (within selected bone area).

709

710 **Electrophysiology**

711 Animals were sacrificed under deep anesthesia and brains removed and placed in ice-
712 cold cutting solution for 1 min (110 mM Choline Chloride, 2.5 mM KCl, 0.5 mM $CaCl_2$,
713 7 mM $MgCl_2$, 1.3 mM NaH_2PO_4, 1.3 mM Na-ascorbate, 0.6 mM Na-pyruvate, 20 mM
714 glucose and 2.5 $NaHCO_3$, 290-310 mOsm/kg, saturated with 95% O_2 and 5% CO_2).
715 Coronal slices (300 μm) were cut using a vibrating microtome (VT1000, Leica), and
716 then allowed to recover for 30 min at 37 °C in artificial cerebral spinal fluid (aCSF, 125
717 mM NaCl, 2.5 mM KCl, 2 mM $CaCl_2$, 1.3 mM $MgCl_2$, 1.3 mM NaH_2PO_4, 1.3 mM Na-
718 ascorbate, 0.6 mM Na-pyruvate, 5 mM glucose, 5mM sucrose and 2.5 mM $NaHCO_3$,
719 300-310 mOsm/kg, saturated with 95% O_2 and 5% CO_2). After recovery, brain slices
720 were transferred to a recording chamber and perfused with 2 ml/min aCSF. Patch
721 pipettes were pulled from borosilicate glass (PG10150-4, World Precision Instruments)
722 and filled with intrapipette solution (35 mM K-gluconate, 10 mM HEPES, 0.2 mM
723 EGTA, 5 mM QX-314, 2 mM Mg-ATP, 0.1 mM Na-GTP, 8 mM NaCl, at 280~290
724 mOsm/kg and adjusted to pH 7.3 with KOH). Whole-cell patch clamp recording of SFO
725 neurons was performed at room temperature (22–25 °C) with a Multiclamp 700B
726 amplifier connected to a Digidata 1440A interface (Axon Instruments). Data were

727 sampled at 10 kHz and analyzed with pClamp10 (Molecular Devices) or MATLAB
728 (MathWorks).
729
730 **Ablation of the sympathetic nerves in the PTG**
731 Sympathetic nervous ablation was performed with 6-hydroxydopamine hydrobromide
732 (6-OHDA, Sigma, H116). Universal ablation of sympathetic nerves was performed in
733 mice by *i.p.* injection of 15 mg/kg 6-OHDA. *In situ* ablation of sympathetic nerves in
734 parathyroid glands of rats was performed by direct injection of 1 μL of 6-OHDA into
735 the parathyroid glands. Calcium tolerance tests were performed 24 hours after 6-OHDA
736 administration.
737
738 **Statistical analysis**
739 In all studies, results were presented as mean ± standard error of the mean (SEM) with
740 n= number of individual animals. Statistical analysis was performed using unpaired
741 Student's t-test for control and treatment comparisons, wherever appropriate, using the
742 statistical program Prism version 7 (GraphPad Software, San Diego, CA, USA). A
743 difference was accepted as statistically significant when probability (P) values were less
744 than 0.05.
745
746
747 **References**

748 1 Wein, M. N. & Kronenberg, H. M. Regulation of Bone Remodeling by Parathyroid Hormone. *Cold*
749 *Spring Harb Perspect Med* **8**, doi:10.1101/cshperspect.a031237 (2018).
750 2 Suarez-Bregua, P., Cal, L., Canestro, C. & Rotllant, J. PTH Reloaded: A New Evolutionary
751 Perspective. *Front Physiol* **8**, 776, doi:10.3389/fphys.2017.00776 (2017).
752 3 Canario, A. V. *et al.* Novel bioactive parathyroid hormone and related peptides in teleost fish. *FEBS*
753 *Lett* **580**, 291-299, doi:10.1016/j.febslet.2005.12.023 (2006).
754 4 Liu, Y. *et al.* Parathyroid hormone gene family in a cartilaginous fish, the elephant shark
755 (Callorhinchus milii). *J Bone Miner Res* **25**, 2613-2623, doi:10.1002/jbmr.178 (2010).
756 5 Suarez-Bregua, P. *et al.* Pth4, an ancient parathyroid hormone lost in eutherian mammals, reveals a
757 new brain-to-bone signaling pathway. *The FASEB Journal* **31**, 569-583 (2016).

6 Dobolyi, A., Palkovits, M. & Usdin, T. B. The TIP39-PTH2 receptor system: unique peptidergic cell groups in the brainstem and their interactions with central regulatory mechanisms. *Progress in neurobiology* **90**, 29-59, doi:10.1016/j.pneurobio.2009.10.017 (2010).
7 Wang, T., Palkovits, M., Rusnak, M., Mezey, E. & Usdin, T. B. Distribution of parathyroid hormone-2 receptor-like immunoreactivity and messenger RNA in the rat nervous system. *Neuroscience* **100**, 629-649, doi:10.1016/s0306-4522(00)00282-7 (2000).
8 Suarez-Bregua, P., Saxena, A., Bronner, M. E. & Rotllant, J. Targeted Pth4-expressing cell ablation impairs skeletal mineralization in zebrafish. *PloS one* **12**, e0186444, doi:10.1371/journal.pone.0186444 (2017).
9 Shoumura, S. *et al.* Origin of autonomic nerve fibers innervating the parathyroid gland in the rabbit. *Acta Anat (Basel)* **115**, 289-295 (1983).
10 Romeo, H. E. *et al.* Origins of the sympathetic projections to rat thyroid and parathyroid glands. *J Auton Nerv Syst* **17**, 63-70 (1986).
11 Mortimer, S. T., Hanley, D. A. & Stell, W. K. Immunohistochemical identification of calcitonin gene-related peptide and substance P in nerves of the bovine parathyroid gland. *Cell Tissue Res* **261**, 339-345 (1990).
12 Egawa, C. & Kameda, Y. Innervation of the chicken parathyroid glands: immunohistochemical study with the TuJ1, galanin, VIP, substance P, CGRP and tyrosine hydroxylase antibodies. *Anat Embryol (Berl)* **191**, 445-450 (1995).
13 Luts, L., Bergenfelz, A., Alumets, J., Luts, A. & Sundler, F. VIP- and PACAP-containing nerve fibers in human parathyroid glands and adenomas: comparison of innervation pattern with animal species. *Ann N Y Acad Sci* **805**, 661-665 (1996).
14 Chen, H., Shoumura, S. & Emura, S. Nerve fibres in the parathyroid gland of the golden hamster (Mesocricetus auratus): immunohistochemical and ultrastructural investigations. *Anat Histol Embryol* **34**, 34-37, doi:10.1111/j.1439-0264.2004.00561.x (2005).
15 Fischer, J. A., Blum, J. W. & Binswanger, U. Acute parathyroid hormone response to epinephrine in vivo. *J Clin Invest* **52**, 2434-2440, doi:10.1172/JCI107434 (1973).
16 Hotta, H., Onda, A., Suzuki, H., Milliken, P. & Sridhar, A. Modulation of calcitonin, parathyroid hormone, and thyroid hormone secretion by electrical stimulation of sympathetic and parasympathetic nerves in anesthetized rats. *Frontiers in neuroscience* **11**, 375 (2017).
17 Chou, F. F., Chen, J. B., Hsieh, K. C. & Liou, C. W. Cognitive changes after parathyroidectomy in patients with secondary hyperparathyroidism. *Surgery* **143**, 526-532, doi:10.1016/j.surg.2007.11.019 (2008).
18 Liu, J. Y. *et al.* Neuropsychologic changes in primary hyperparathyroidism after parathyroidectomy from a dual-institution prospective study. *Surgery*, doi:10.1016/j.surg.2020.06.006 (2020).
19 McKinley, M. J. *et al.* The sensory circumventricular organs of the mammalian brain. *Adv Anat Embryol Cell Biol* **172**, III-XII, 1-122, back cover, doi:10.1007/978-3-642-55532-9 (2003).
20 Joborn, C. *et al.* Cerebrospinal fluid calcium, parathyroid hormone, and monoamine and purine metabolites and the blood-brain barrier function in primary hyperparathyroidism. *Psychoneuroendocrinology* **16**, 311-322 (1991).
21 Zimmerman, C. A., Leib, D. E. & Knight, Z. A. Neural circuits underlying thirst and fluid homeostasis. *Nature Reviews Neuroscience* **18**, 459 (2017).
22 Oka, Y., Ye, M. & Zuker, C. S. Thirst driving and suppressing signals encoded by distinct neural populations in the brain. *Nature* **520**, 349 (2015).
23 Vivas, L., Chiaraviglio, E. & Carrer, H. F. Rat organum vasculosum laminae terminalis in vitro: responses to changes in sodium concentration. *Brain Res* **519**, 294-300, doi:10.1016/0006-8993(90)90091-o (1990).
24 Anderson, J. W., Washburn, D. L. & Ferguson, A. V. Intrinsic osmosensitivity of subfornical organ neurons. *Neuroscience* **100**, 539-547, doi:10.1016/s0306-4522(00)00313-4 (2000).
25 Zimmerman, C. A. *et al.* Thirst neurons anticipate the homeostatic consequences of eating and drinking. *Nature* **537**, 680 (2016).
26 Matsuda, T. *et al.* Distinct neural mechanisms for the control of thirst and salt appetite in the subfornical organ. *Nature neuroscience* **20**, 230 (2017).
27 Nation, H. L., Nicoleau, M., Kinsman, B. J., Browning, K. N. & Stocker, S. D. DREADD-induced activation of subfornical organ neurons stimulates thirst and salt appetite. *Journal of neurophysiology* **115**, 3123-3129 (2016).
28 Dobolyi, A., Dimitrov, E., Palkovits, M. & Usdin, T. B. The neuroendocrine functions of the parathyroid hormone 2 receptor. *Front Endocrinol (Lausanne)* **3**, 121, doi:10.3389/fendo.2012.00121 (2012).
29 Dimitrov, E. L., Kuo, J., Kohno, K. & Usdin, T. B. Neuropathic and inflammatory pain are

818 modulated by tuberoinfundibular peptide of 39 residues. *Proc Natl Acad Sci U S A* **110**, 13156-13161,
819 doi:10.1073/pnas.1306342110 (2013).
820 30 Tsuda, M. C., Yeung, H. M., Kuo, J. & Usdin, T. B. Incubation of Fear Is Regulated by TIP39
821 Peptide Signaling in the Medial Nucleus of the Amygdala. *J Neurosci* **35**, 12152-12161,
822 doi:10.1523/JNEUROSCI.1736-15.2015 (2015).
823 31 Dimitrov, E. L., Petrus, E. & Usdin, T. B. Tuberoinfundibular peptide of 39 residues (TIP39)
824 signaling modulates acute and tonic nociception. *Exp Neurol* **226**, 68-83,
825 doi:10.1016/j.expneurol.2010.08.004 (2010).
826 32 Faber, C. A., Dobolyi, A., Sleeman, M. & Usdin, T. B. Distribution of tuberoinfundibular peptide
827 of 39 residues and its receptor, parathyroid hormone 2 receptor, in the mouse brain. *Journal of*
828 *Comparative Neurology* **502**, 563-583 (2007).
829 33 Munger, J. S. & Sheppard, D. Cross talk among TGF-β signaling pathways, integrins, and the
830 extracellular matrix. *Cold Spring Harbor perspectives in biology* **3**, a005017 (2011).
831 34 Policeni, B. A., Smoker, W. R. & Reede, D. L. in *Seminars in Ultrasound, CT and MRI.* 104-114
832 (Elsevier).
833 35 Bain, V. E. *et al.* Tissue-specific roles for sonic hedgehog signaling in establishing thymus and
834 parathyroid organ fate. *Development* **143**, 4027-4037 (2016).
835 36 Jendryka, M. *et al.* Pharmacokinetic and pharmacodynamic actions of clozapine-N-oxide, clozapine,
836 and compound 21 in DREADD-based chemogenetics in mice. *Scientific reports* **9**, 1-14 (2019).
837 37 Usdin, T., Hoare, S., Wang, T., Mezey, E. & Kowalak, J. TIP39: a new neuropeptide and PTH2-
838 receptor agonist from hypothalamus. *Nature neuroscience* **2**, 941 (1999).
839 38 Joborn, C., Hetta, J., Palmer, M., Akerstrom, G. & Ljunghall, S. Psychiatric symptomatology in
840 patients with primary hyperparathyroidism. *Ups J Med Sci* **91**, 77-87 (1986).
841 39 Kollars, J. *et al.* Primary hyperparathyroidism in pediatric patients. *Pediatrics* **115**, 974-980,
842 doi:10.1542/peds.2004-0804 (2005).
843 40 Roman, S. A. *et al.* The effects of serum calcium and parathyroid hormone changes on
844 psychological and cognitive function in patients undergoing parathyroidectomy for primary
845 hyperparathyroidism. *Ann Surg* **253**, 131-137, doi:10.1097/SLA.0b013e3181f66720 (2011).
846 41 Driessen, M., Wetterling, T., Wedel, T. & Preuss, R. Secondary hyperparathyroidism and depression
847 in chronic renal failure. *Nephron* **70**, 334-339, doi:10.1159/000188614 (1995).
848 42 Fegley, D. *et al.* Increased fear - and stress - related anxiety - like behavior in mice lacking
849 tuberoinfundibular peptide of 39 residues. *Genes, Brain and Behavior* **7**, 933-942 (2008).
850 43 Swanson, L. W. & Sawchenko, P. E. Hypothalamic integration: organization of the paraventricular
851 and supraoptic nuclei. *Annu Rev Neurosci* **6**, 269-324, doi:10.1146/annurev.ne.06.030183.001413 (1983).
852 44 Kawabe, T., Chitravanshi, V. C., Kawabe, K. & Sapru, H. N. Cardiovascular function of a
853 glutamatergic projection from the hypothalamic paraventricular nucleus to the nucleus tractus solitarius
854 in the rat. *Neuroscience* **153**, 605-617 (2008).
855 45 Shi, Z. *et al.* Leptin increases sympathetic nerve activity via induction of its own receptor in the
856 paraventricular nucleus. *Elife* **9**, e55357 (2020).
857 46 Baldock, P. A. *et al.* Neuropeptide Y Attenuates Stress-Induced Bone Loss Through Suppression of
858 Noradrenaline Circuits. *journal of bone and mineral research* **29**, 2238-2249, doi:10.1002/JBMR.2205
859 (2014).
860 47 Paxinos, G. & Franklin, K. B. J. *Paxinos and Franklin's the Mouse Brain in Stereotaxic Coordinates*.
861 (2012).
862 48 Lowery, R. L. & Majewska, A. K. Intracranial injection of adeno-associated viral vectors. *JoVE*
863 *(Journal of Visualized Experiments)*, e2140 (2010).
864 49 Kondoh, K. *et al.* A specific area of olfactory cortex involved in stress hormone responses to
865 predator odours. *Nature* **532**, 103-106 (2016).

866

Acknowledgements

This project was partly supported by the National Natural Science Foundation of China (82072489); Key Research Program of Frontier Sciences of Chinese Academy of Sciences (QYZDB-SSW-SMC056); Shenzhen Governmental Basic Research Grant (JCYJ20180507182301299).

Author contributions:

Fan Yang and William W Lu supervised the study. Lu Zhang, Nian Liu designed the experiments and conducted chemogenetic experiments, animal behavior studies, serum biochemical analysis and analyzed data. Jie Shao performed electrophysiological recordings in brain slices. Dashuang Gao performed PRV retrograde tracing experiments. Yunhui Liu performed sympathetic nerve ablation test.

Declaration of interests: The authors have declared that no conflict of interest exists.

884 **Figures**

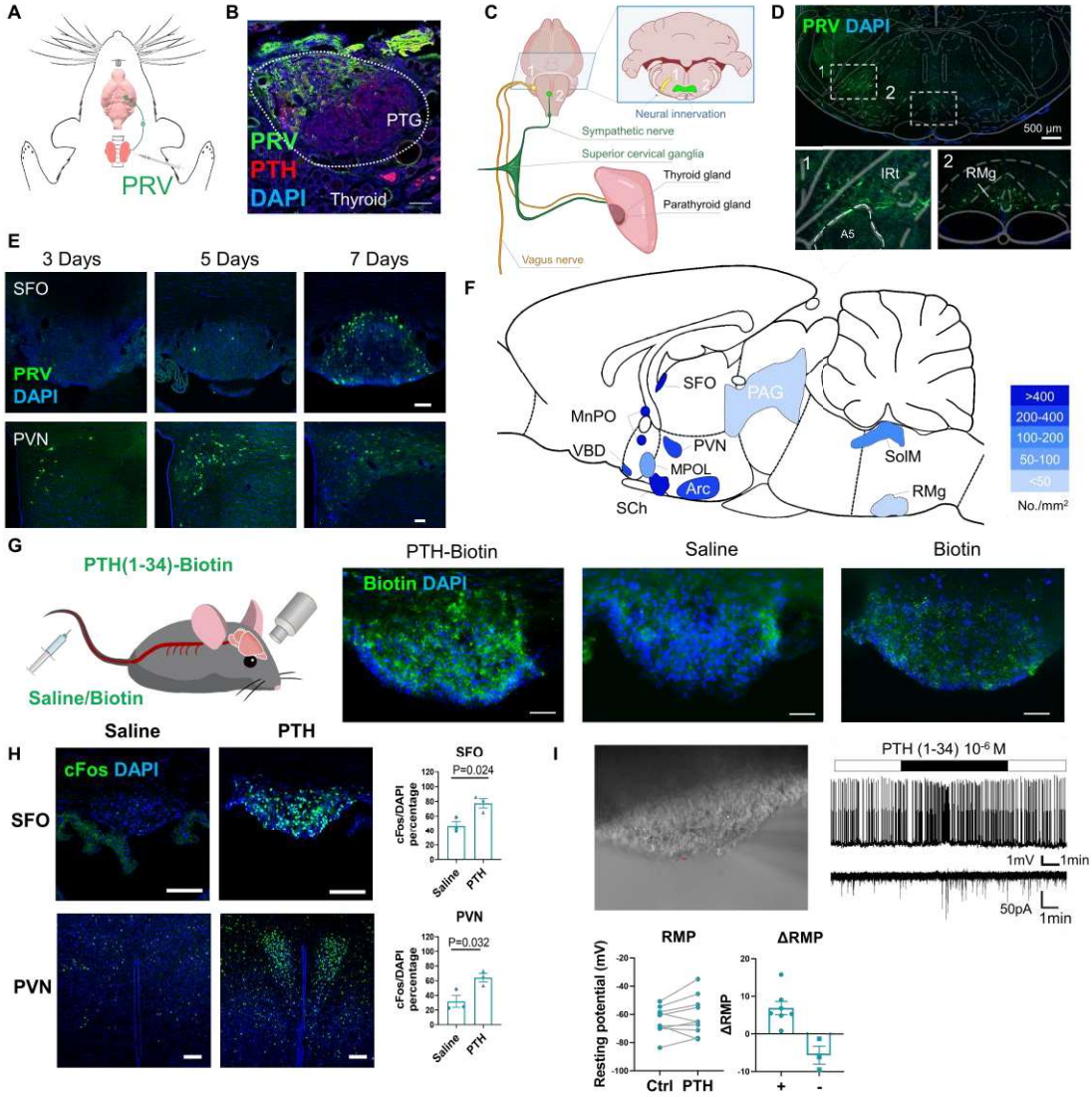

885

886 **Figure 1. Parathyroid glands are connected to the SFO and PVN.**

887 **A,** Schematic showing pseudorabies virus (PRV) infection of SD rat parathyroid gland
888 (PTG) and poly trans-synaptic connection to the central nervous system. **B,** PRV *in situ*
889 expression within rat PTG. Scale bar, 50 μm. **C,** Schematic showing the peripheral
890 neural innervation of the parathyroid glands and the connection ends to brain stem. **D,**
891 PRV expression in brain stem 3 days after administration to the rat parathyroid gland.
892 IRt, intermediate reticular nucleus; RMg, raphe magnus nucleus. **E,** PRV expression in
893 subfornical organ (SFO, ***upper,*** scale bar, 100 μm) and paraventricular nucleus (PVN,

894 ***lower,*** scale bar, 100 μm) at 3, 5 and 7 days after injection into the rat parathyroid gland.
895 **F,** PRV expression density in different rat brain areas after PRV neural tracing (No./mm^2,
896 n=3). Arc, arcuate nucleus; MnPO, median preoptic nucleus; MPOL, medial preoptic
897 nucleus, lateral part; SolM, nucleus tractus solitarius; PAG, periaqueductal gray; PVN,
898 paraventricular thalamic nucleus; RMg, raphe magnus nucleus; SFO, subfornical organ;
899 SCh, suprachiasmatic nucleus; VDB, nucleus of the vertical limb of the diagonal band.
900 **G**, Peripheral administrated PTH-biotin binding to the SFO. ***Left,*** Schematic showing
901 peripheral administration of saline, biotin and PTH-biotin to C57 mice. ***Right***,
902 Immunofluorescence staining of biotin in SFO of C57 mice. Scale bar, 100 μm. **H**,
903 CFos expression in the SFO (***upper,*** scale bar, 100 μm) and PVN (***lower,*** scale bar, 100
904 μm) after peripheral PTH administration. ***Right bar chart***, Quantification of cFos
905 positive cells in the SFO and PVN (n=3). **I**, Electrophysiological recording of SFO cells
906 with whole-cell patch (n=8). ***Upper,*** representative electrophysiological whole-cell
907 patch recording of SFO neurons responses to PTH (scale bar, 2μm); ***lower***, statistical
908 analysis of changes in resting membrane potential during PTH stimulation. RPM,
909 resting membrane potential, P analyzed by unpaired two-tailed t-test. All error bars and
910 shaded areas show mean ± s.e.m. DAPI, 4',6-diamidino-2-phenylindole,
911 dihydrochloride.

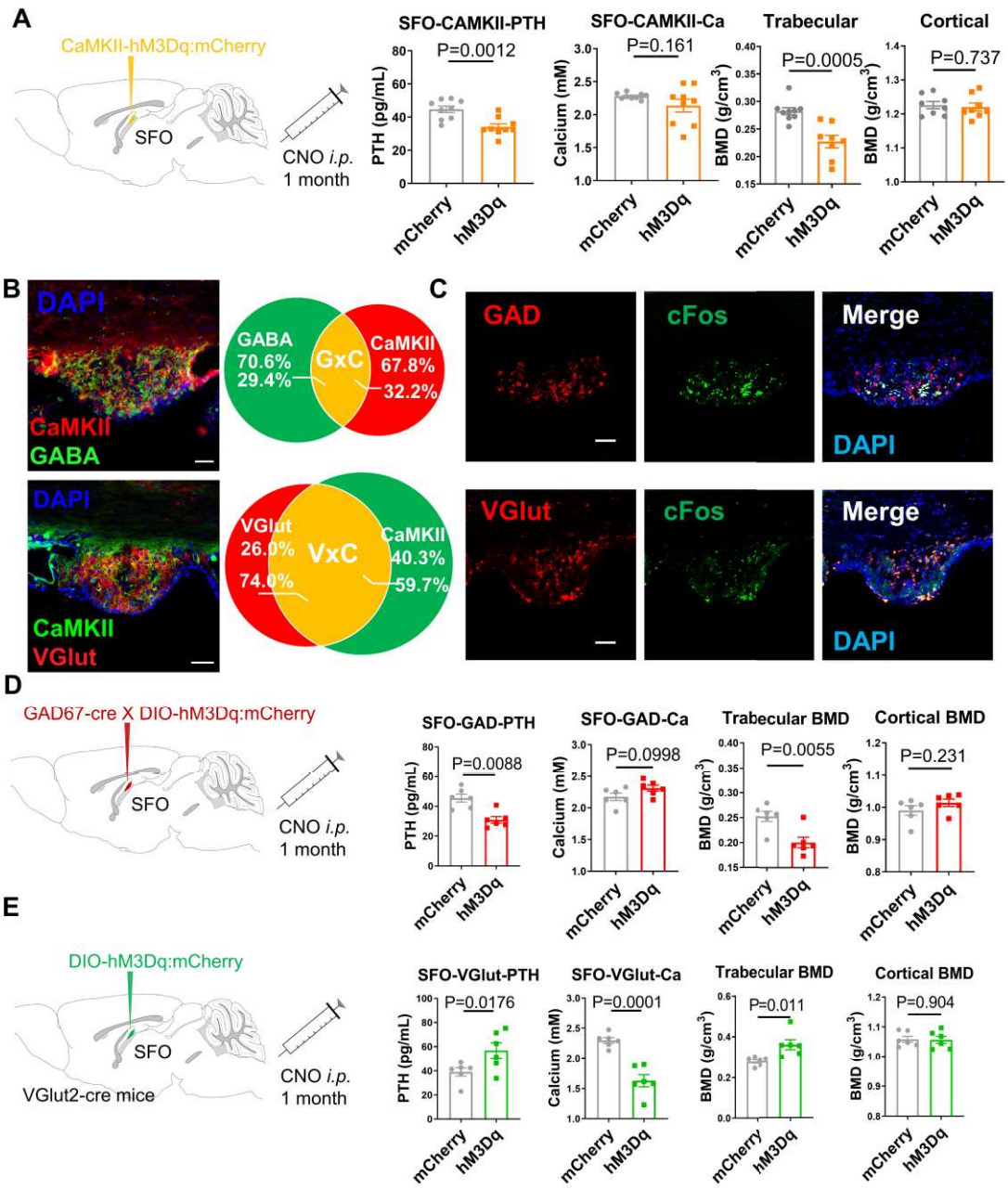

Figure 2. SFO neurons regulate serum PTH level.

A, Chemogenetic stimulation of Calcium/calmodulin-dependent protein kinase II (CaMKII) neurons in the subfornical organ (SFO) of C57 mice (n=9). ***Left***, injection of AAV-CaMKII-hM3Dq/mCherry into the SFO of C57 mice followed by 1-month clozapine-N-oxide (CNO) *i.p*. administration. ***Right bar charts***, serum PTH level, total serum calcium level, tibia trabecular bone mineral density (BMD), and femur cortical BMD from MicroCT analysis. **B**, ***Upper left***, Immunofluorescence (IF) staining of

920 CaMKII and gamma-aminobutyric acid (GABA) in the SFO of C57 mice. Scale bar,
921 100 μm. ***Lower left***, IF staining of CaMKII colocalized with mCherry in the SFO of
922 VGlut2-cre mice transfected with AAV-DIO-mCherry in SFO. Scale bar, 100 μm.
923 ***Upper right***, statistical analysis of GABA and CaMKII colocalization (n=3 mice).
924 ***Lower right***, statistical analysis of VGlut and CaMKII colocalization (n=3 mice). **C**, *In*
925 *situ* hybridization of *Gad1/2* and *Vglut2* mRNA in the SFO colocalized with IF staining
926 of cFos after *i.v.* PTH stimulation in C57 mice. Scale bar, 50 μm. **D**, Chemogenetic
927 stimulation of GABAergic neurons in the SFO of C57 mice (n=6 mice). ***Left***, injection
928 of AAV-GAD67-cre and AAV-DIO-hM3Dq/mCherry mixture into the SFO of C57 mice
929 followed with 1-month CNO *i.p.* administration; ***Right bar charts***, serum PTH level,
930 total serum calcium level, tibia trabecular BMD, and femur cortical BMD in MicroCT
931 analysis. **E**, Chemogenetic stimulation of glutamatergic neurons in the SFO of VGlut2-
932 cre mice (n=6 mice). ***Left***, injection of AAV-DIO-hM3Dq/mCherry into the SFO of
933 VGlut2-cre mice followed with 1- month CNO *i.p.* administration; ***Right bar charts***,
934 serum PTH, total serum calcium level, tibia trabecular BMD, femur cortical BMD from
935 MicroCT analysis. P analyzed by unpaired two-tailed t-test. All error bars and shaded
936 areas show mean ± s.e.m. GAD, glutamic acid decarboxylase; VGlut, vesicular
937 glutamate transporter; DAPI, 4',6-diamidino-2-phenylindole, dihydrochloride.

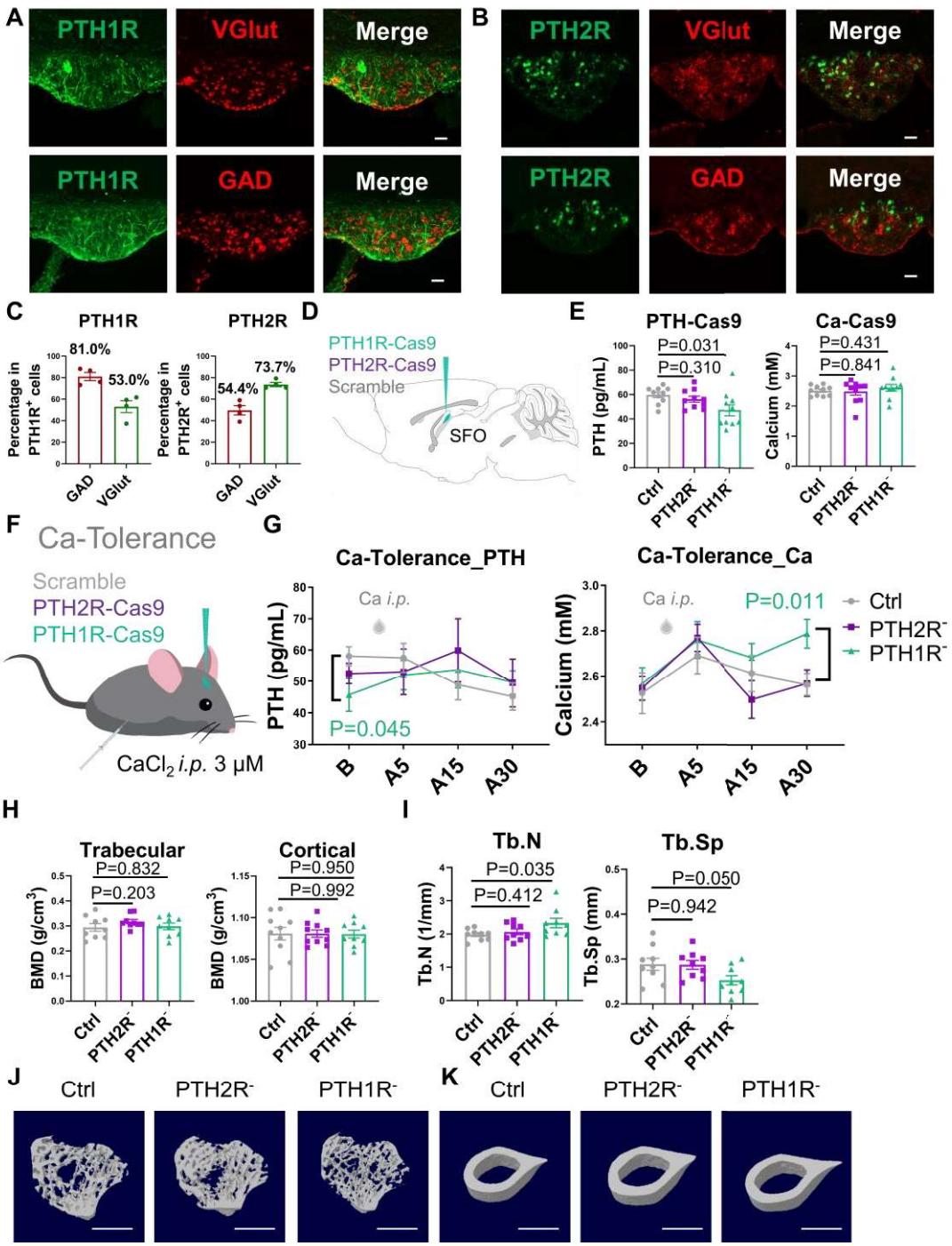

938

939 **Figure 3. The function of PTH1R and PTH2R in the SFO.**

940 **A**, *Gad1/2* and *Vglut2* mRNA expression colocalized with immunofluorescence
941 staining of PTH1R and PTH2R in the SFO of C57 mice (scale bar, 50 μm). **B,** *Gad1/2*
942 and *Vglut2* mRNA expression colocalized with PTH2R cells in the SFO of PTH2R-
943 creER^{T2} mice (scale bar, 50 μm). **C**, Statistical analysis of colocalized cells in **A** and **B**
944 (n=4 mice, scale bar, 50 μm). (**D-E)** Serum PTH and calcium changes after knockdown

945 of PTH1R/PTH2R in SFO. **D**, Schematic showing the injection of LV-PTH1R-Cas9
946 (PTH1R^{-}) or LV-PTH2R-Cas9 (PTH2R^{-}) or LV-Scramble (Ctrl) into the SFO of C57
947 mice. **E**, Basic serum PTH and calcium level of C57 mice after knockdown of
948 PTH1R/PTH2R in SFO respectively (n=10 mice). **(F-G)**, Calcium tolerance tests in
949 C57 mice after knockdown of PTH1R/PTH2R in the SFO (n=10 mice). **F**, Schematic
950 showing the knockdown of PTH1R/PTH2R, and serum was collected before and 5, 15,
951 30 mins after injection of $CaCl_2$ (3μM, *i.p.*). **G**, ***Left***, serum PTH before and after *i.p.*
952 injection of $CaCl_2$ in control, SFO^{pth1r-} and SFO^{pth2r-} groups (n=10 mice); ***right***, serum
953 calcium after *i.p.* injection of $CaCl_2$. in control, SFO^{pth1r-} and SFO^{pth2r-} groups, (n=10
954 mice). **H**, Tibia trabecular bone mineral density (BMD) and femur cortical BMD
955 assessed from MicroCT of C57 mice after knockdown of PTH1R/PTH2R in the SFO
956 (n=9 mice). **I**, Trabecular numbers (Tb.N) and trabecular separation (Tb.Sp) of C57
957 mice tibia after knockdown of PTH1R/PTH2R (n=9 mice). (**J-K**), 3D reconstruction of
958 MicroCT analysis of tibia trabecular (**J**) and femur cortical (**K**) bones in ctrl/PTH2R^{-}
959 /PTH1R^{-} groups (scale bar, 1 mm). P values were analyzed by unpaired two-tailed t-
960 test. All error bars and shaded areas show mean ± s.e.m. VGlut, vesicular glutamate
961 transporter; GAD, glutamate decarboxylase.
962

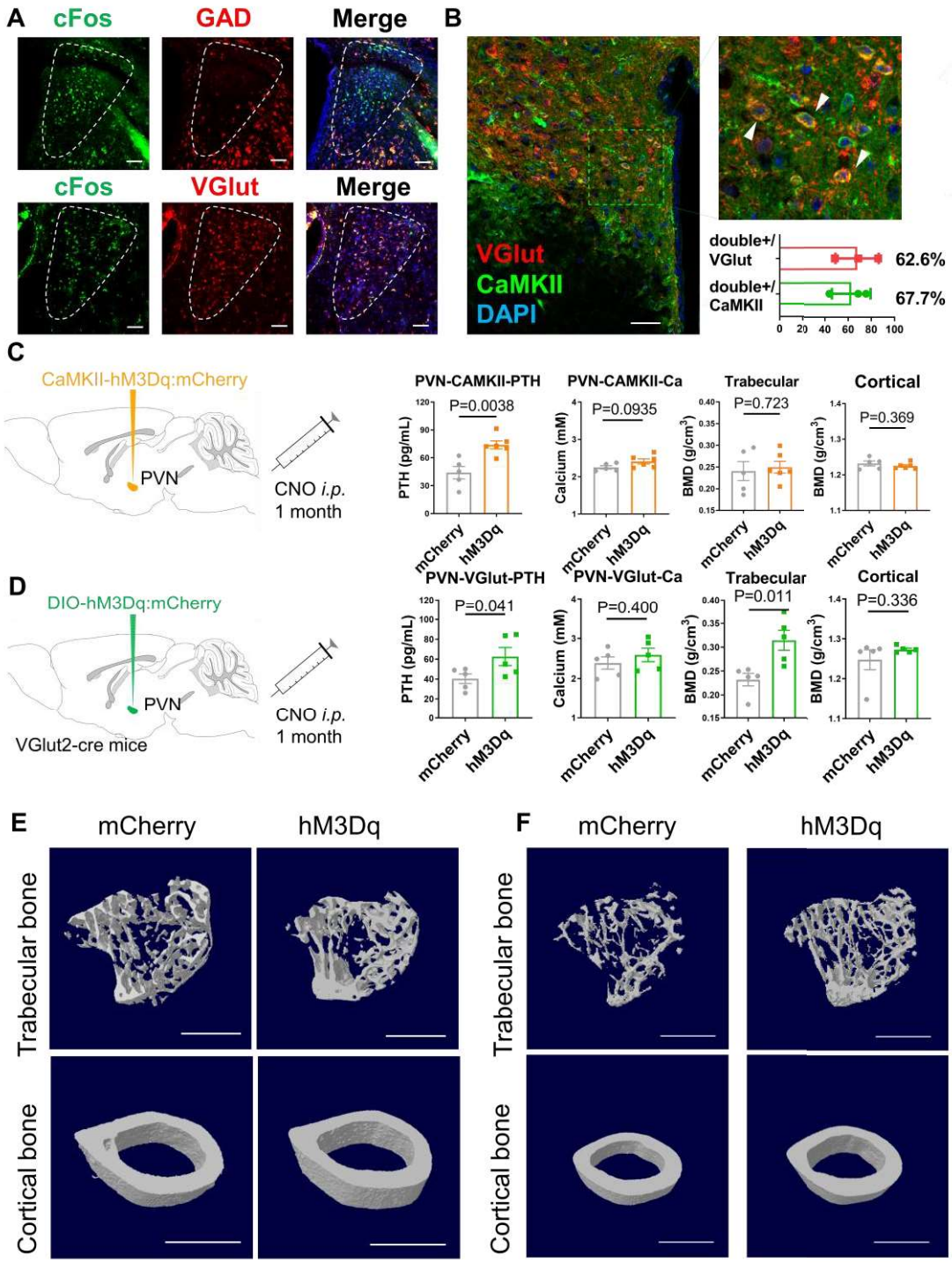

963

964 **Figure 4. PVN neurons regulate serum PTH level.**

965 **A**, *In situ* hybridization of GAD1/2 and VGlut2 mRNA in the paraventricular nucleus

966 (PVN) colocalized with cFos staining after *i.v.* PTH stimulation. Scale bar, 100 μm. **B**,

967 ***Left and upper right***, colocalization of VGlut and CaMKII markers in the PVN of

968 VGlut2-cre mice (scale bar, 100 μm); ***lower right***, statistical analysis of the colocalized

969 cells (n=3 mice). **C**, Chemogenetic activation of CaMKII neurons in the PVN of C57
970 mice (n=5-6 mice). ***Left***, schematic showing the injection of AAV-CaMKII-
971 hM3Dq/mCherry into the PVN of C57 mice followed with 1-month CNO *i.p.*
972 administration. ***Right bar charts***, serum PTH, total serum calcium level, tibia trabecular
973 bone mineral density (BMD), and femur cortical BMD from MicroCT analysis. **D**,
974 Chemogenetic stimulation of VGlut neurons in the PVN of VGlut2-cre mice (n=6 mice).
975 ***Left***, schematic showing the injection of AAV-DIO-hM3Dq/mCherry into the PVN of
976 VGlut2-cre mice followed with 1-month CNO *i.p.* administration; ***Right bar charts***,
977 serum PTH, total serum calcium level, tibia trabecular BMD, and femur cortical BMD
978 from MicroCT analysis. **E,** 3D reconstruction of MicroCT analysis of tibia trabecular
979 bone and femur cortical bone in C57 mice transfected with CaMKII-mCherry or
980 CaMKII-hM3Dq-mCherry in the PVN and then administrated with CNO for 1 month
981 (scale bar, 1 mm). **F**, 3D reconstruction of MicroCT result of tibia trabecular bone and
982 femur cortical bone in VGlut2-cre mice transfected with DIO-hM3Dq-mCherry or
983 DIO-mCherry in PVN and administrated with CNO for 1 month. Scale bar, 1 mm. P
984 analyzed by unpaired two-tailed t-test. All error bars and shaded areas show mean ±
985 s.e.m. CNO, clozapine-N-oxide.

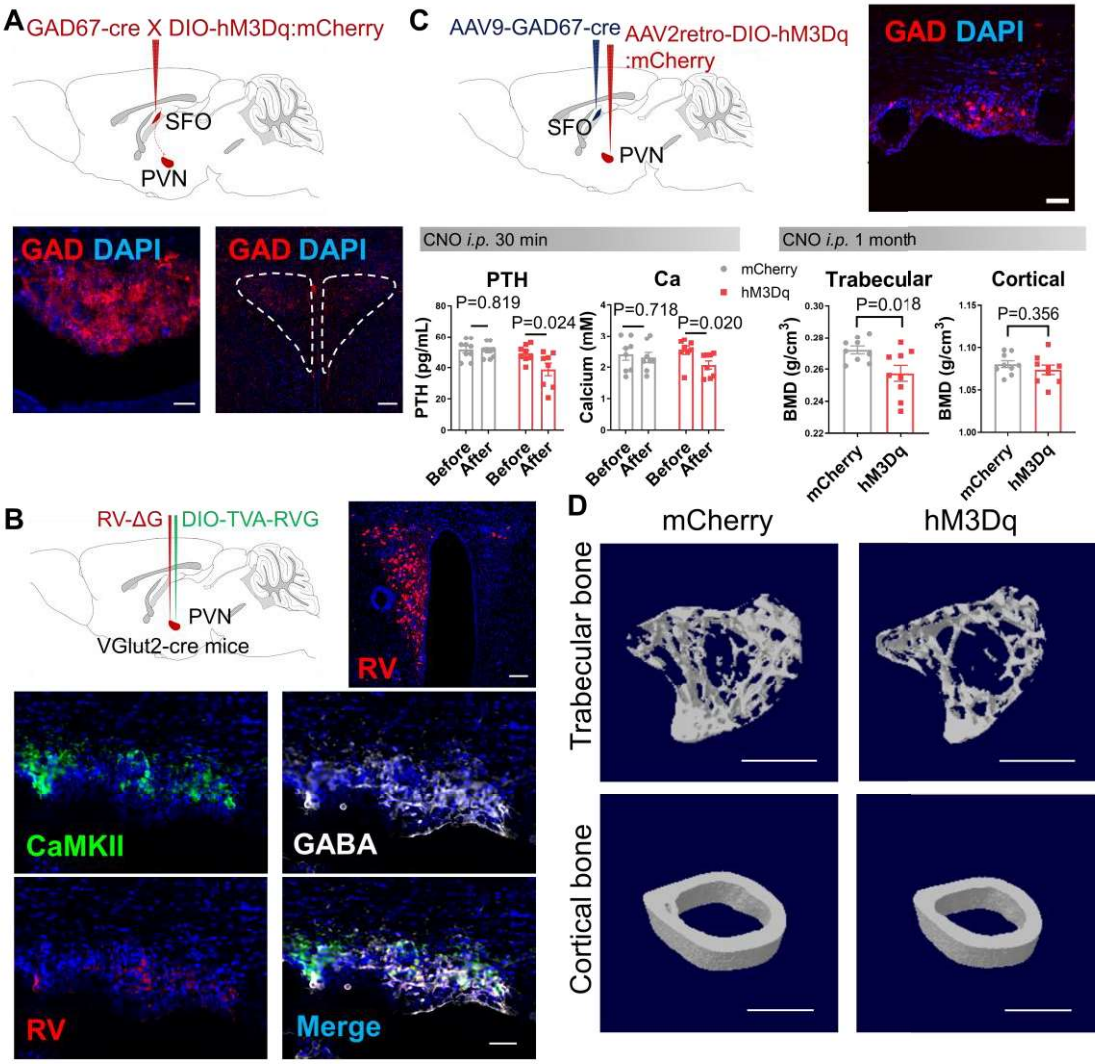

986

987 **Figure 5. SFO^{GAD} neurons send projections to the PVN.**

988 **A**, ***Upper***, schematic showing the injection of AAV-GAD67-cre and AAV-DIO-
989 mCherry mixture into the SFO of C57 mice; ***lower***, GABAergic neural projections
990 observed from the SFO (***left***, scale bar, 50 μm) to the PVN (***right***, scale bar, 100 μm).
991 **B**, ***Upper left***, schematic showing injection of AAV9-DIO-TVA-RVG and then RV-ΔG-
992 dsRed into the PVN of VGlut2-cre mice; ***upper right***, genetically modified rabies virus
993 (RV) tracing from PVN^{VGlut} neurons (scale bar, 100 μm). ***Middle and lower***,
994 colocalization of RV signals with IF staining of CaMKII and GABA signals in SFO
995 (scale bar, 50 μm). (**C-D**) Chemogenetic activation of SFO^{GAD}→PVN neural
996 projections in C57 mice (n=9 mice). **C**, ***Upper left***, schematic showing injection of

997 AAV-GAD67-cre into the SFO and AAV2retro-DIO-hM3Dq/mCherry into the PVN of
998 C57 mice followed with 1-month CNO *i.p.* administration. ***Upper right,*** mCherry
999 signals observed in the SFO indicating GAD67^{+} neurons with axon terminals projected
1000 to PVN (scale bar, 50 μm). ***Lower left***, serum PTH before and 30 min after CNO
1001 injection, total serum calcium level before and 30 min after *i.p.* CNO injection into
1002 mCherry group and hM3Dq group. ***Lower right***, tibia trabecular BMD and femur
1003 cortical BMD in MicroCT analysis after 1-month CNO administration into mCherry
1004 group and hM3Dq group. **D**, 3D reconstruction of MicroCT analysis of tibia trabecular
1005 bone and femur cortical bone in C57 mice injected with GAD67-cre virus in the SFO
1006 and DIO-mCherry or DIO-hM3Dq-mCherry in the PVN and then given CNO for 1
1007 month. Scale bar, 1 mm. P analyzed by paired two-tailed t-test for before-after analysis,
1008 unpaired two-tailed t-test for mCherry-hM3Dq analysis. All error bars and shaded areas
1009 show mean ± s.e.m.
1010
1011

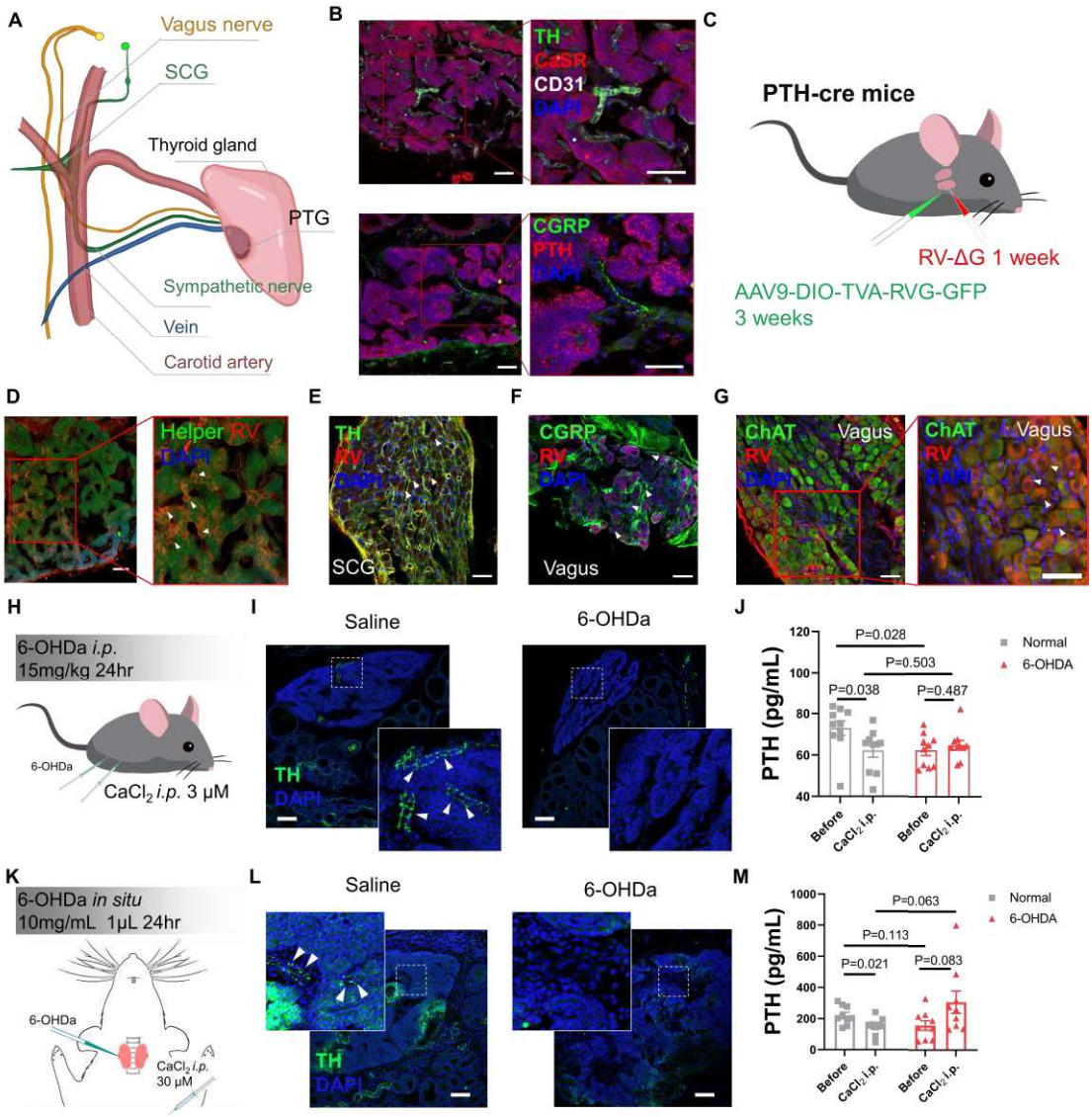

Figure 6. Peripheral innervation in parathyroid glands and sympathetic regulation of PTH.

A, Schematic demonstration of the anatomical relationship between parathyroid gland (PTG) and the surrounding peripheral nerves and blood vessels. PTG, parathyroid gland; SCG, superior cervical ganglia. **B,** Innervation and location of tyrosine hydroxylase (TH) sympathetic nerves, CD31 capillaries and calcitonin gene-related peptide (CGRP) sensory nerves in mice parathyroid glands. Scale bar, 50 μm. **C**, Schematic showing helper (AAV-DIO-TVA-RVG-GFP) and rabies virus (RV-ΔG-dsRed) infection of the parathyroid gland in PTH-cre mice and trans-monosynaptic connection to the

1022 peripheral nervous system. (**D-G**), Neural specific rabies virus (RV) tracing from mice
1023 parathyroid glands to the superior cervical ganglion (SCG) and the inferior ganglion of
1024 vagus nerve (Vagus). **D**, *In situ* RV (red) and helper (green) expression in the
1025 parathyroid gland of PTH-cre mice. White arrow indicates colocalization of RV
1026 expression and helper signals. Scale bar, 50 μm. **E**, RV signals colocalized with IF
1027 staining of TH expression in mice SCG. **F**, RV signals colocalized with IF staining of
1028 CGRP expression in the vagus ganglion. **G**, RV signals colocalized with IF staining of
1029 ChAT expression in the vagus ganglion. White arrow indicates colocalization of RV
1030 signals with TH/ChAT/CGRP signals. Scale bar, 50 μm. (**H-J**), Calcium tolerance study
1031 in C57 mice of universal ablation of sympathetic nerves. **H**, Schematic showing
1032 administration of 6-OHDa (15 mg/kg, *i.p.*) to ablate the sympathetic terminals and
1033 calcium tolerance test was performed 24hrs after 6-OHDa injection. **I**, IF staining of
1034 TH indicates that sympathetic nerve innervation in mice PTG were ablated 24hrs after
1035 6-OHDa administration. Scale bar, 100 μm. **J,** Serum PTH levels before and 30 mins
1036 after *i.p.* administration of $CaCl_2$ in C57 mice with or without sympathetic nerve
1037 ablation by 6-OHDA (n=10 mice). P analyzed by two-way ANOVA test comparing the
1038 6-OHDa effects among different groups. (**K-M**), Calcium tolerance study in SD rat of
1039 PTG after local ablation of sympathetic nerves. **K**, Schematic showing local injection
1040 of 6-OHDa (10 mg/mL, 1μL) to ablate the sympathetic nerve in rat parathyroid glands
1041 and then calcium tolerance test was performed 24hrs after 6-OHDa injection. **L**, IF
1042 staining of TH indicating sympathetic nerve innervation in rat PTG were ablated 24hrs
1043 after 6-OHDa administration. Scale bar, 100 μm **M,** Serum PTH before and 30 mins
1044 after *i.p.* administration of $CaCl_2$ in rats with or without sympathetic nerve ablation by
1045 6-OHDA (n=9 rats). The P value were analyzed by unpaired two-tailed t-test. All error
1046 bars and shaded areas show mean ± s.e.m. 6-OHDA, 6-hydroxydopamine; CaSR,

1047 calcium sensory receptor; CD31, cluster of differentiation 31; CGRP, calcitonin-gene
1048 related protein; ChAT, choline acetyltranserase; PTG, parathyroid gland; SCG, superior
1049 cervical ganglia; TH, tyrosine hydroxylase.
1050
1051
1052
1053
1054
1055
1056
1057
1058
1059
1060
1061
1062
1063
1064
1065
1066
1067
1068
1069

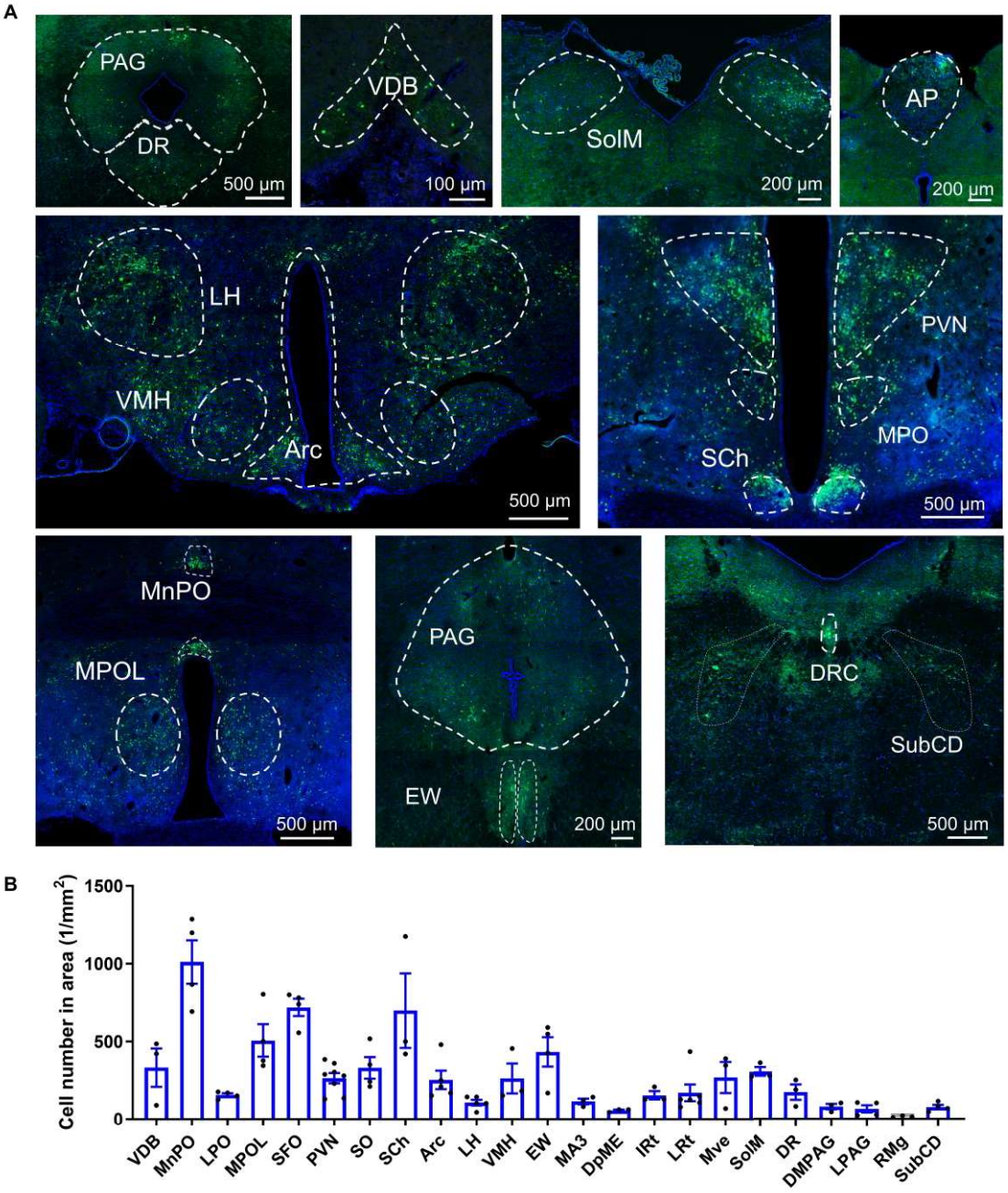

1070

1071 **Supplementary figure 1. Poly-synaptic retrograde PRV labeling of specific rat**

1072 **brain nuclei**

1073 **A**, Pseudorabies virus (PRV) retrograde tracing from rat PTG to different brain nuclei,

1074 including: the AP, area postrema; Arc, arcuate nucleus; DMPAG, dorsomedial

1075 periaqueductal gray; DpME, deep mesencephalic nucleus; DR, dorsal raphe nucleus;

1076 EW, edinger-westphal nucleus; IRt, intermediate reticular nucleus; LH, lateral

1077 hypothalamic area; LPAG, lateral periaqueductal gray; LPO, lateral preoptic area; MA3,

1078 medial accessory oculomotor nucleus; MnPO, median preoptic nucleus; MPOL, medial
1079 preoptic nucleus, lateral part; Mve, medial vestibular nucleus; PVN, paraventricular
1080 thalamic nucleus; RMg, raphe magnus nucleus; SCh, suprachiasmatic nucleus, lateral
1081 part; SFO, subfornical organ; SO, supraoptic nucleus; SolM, nucleus of the solitary
1082 tract, medial part; SubCD, subcoeruleus nucleus, dorsal part; VDB, nucleus of the
1083 vertical limb of the diagonal band; VMH, ventromedial hypothalamic nucleus. N=3 rats.
1084 **B**, Statistical analysis of signal density of different brain nuclei 7 days after PRV
1085 injection from rat PTG. All error bars and shaded areas show mean ± s.e.m.
1086

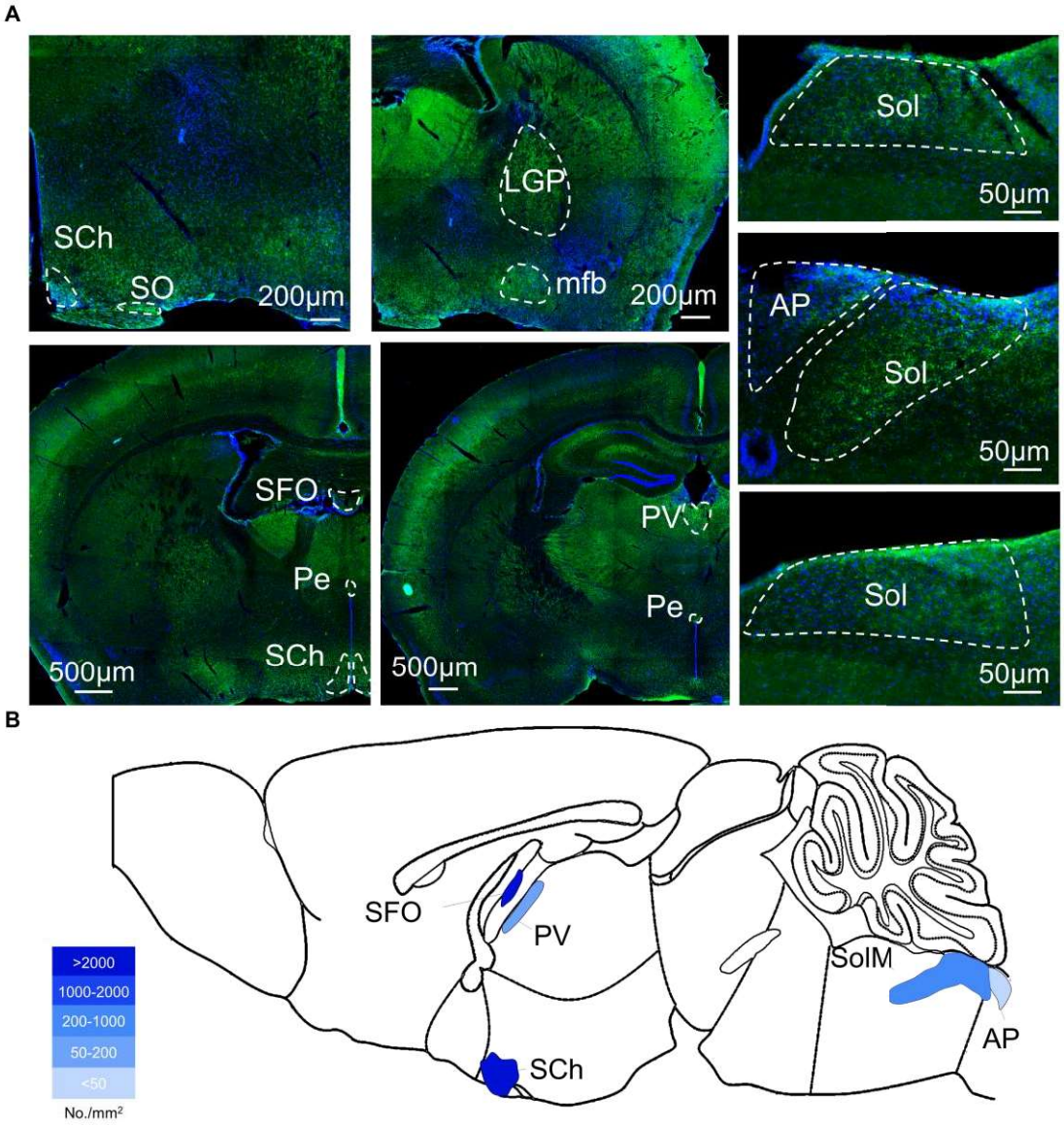

1087

1088 **Supplementary figure 2. PTH-biotin binding to specific brain nuclei after**
1089 **peripheral *i.v.* administration.**
1090 **A**, Immunofluorescence staining of biotin indicating the PTH-biotin binds to different
1091 nuclei in the C57 mouse brain, including: the AP, area postrema; LGP, lateral globus
1092 pallidus; mfb, medial forebrain bundle; Pe, periventricular hypothalamic nucleus; PV,
1093 periventricular fiber system; SCh, suprachiasmatic nucleus; SFO, subfornical organ;
1094 SO, supraoptic nucleus; Sol, solitary tract. **B**, PTH-biotin binding nuclei location and
1095 the signal density (n=3 mice).
1096

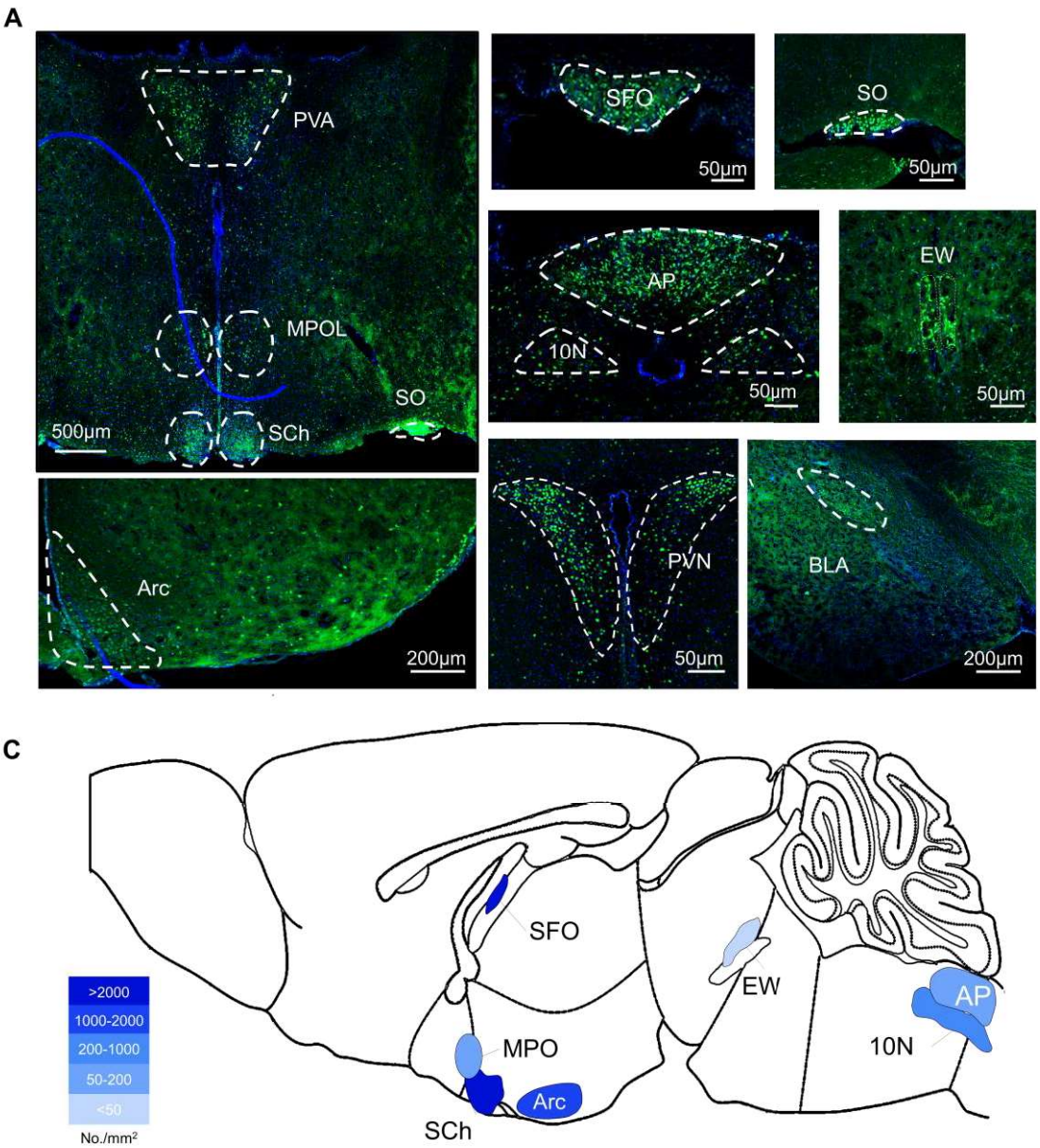

1097

1098 **Supplementary figure 3. cFos expression in the mouse brain after peripheral *i.v.***

1099 **PTH stimulation.**

1100 **A**, Immunofluorescence staining of cFos (green) were observed in specific brain nuclei

1101 including: the 10N, dorsal motor nucleus of vagus; Arc, arcuate hypothalamic nucleus;

1102 AP, area postrema; BLA, basolateral amygdaloid nucleus, anteriorpart; EW, Edinger-

1103 Westphal nucleus; MPOL, medial preoptic nucleus, lateral part; PVA, paraventricular

1104 thalamic nucleus, anterior part; PVN, paraventricular thalamic nucleus; SCh,

1105 suprachiasmatic nucleus; SFO, subfornical organ; SO, supraoptic nucleus. **B**, Locations

1106 of PTH-responding nuclei and relative cFos expression density (n=3 mice).

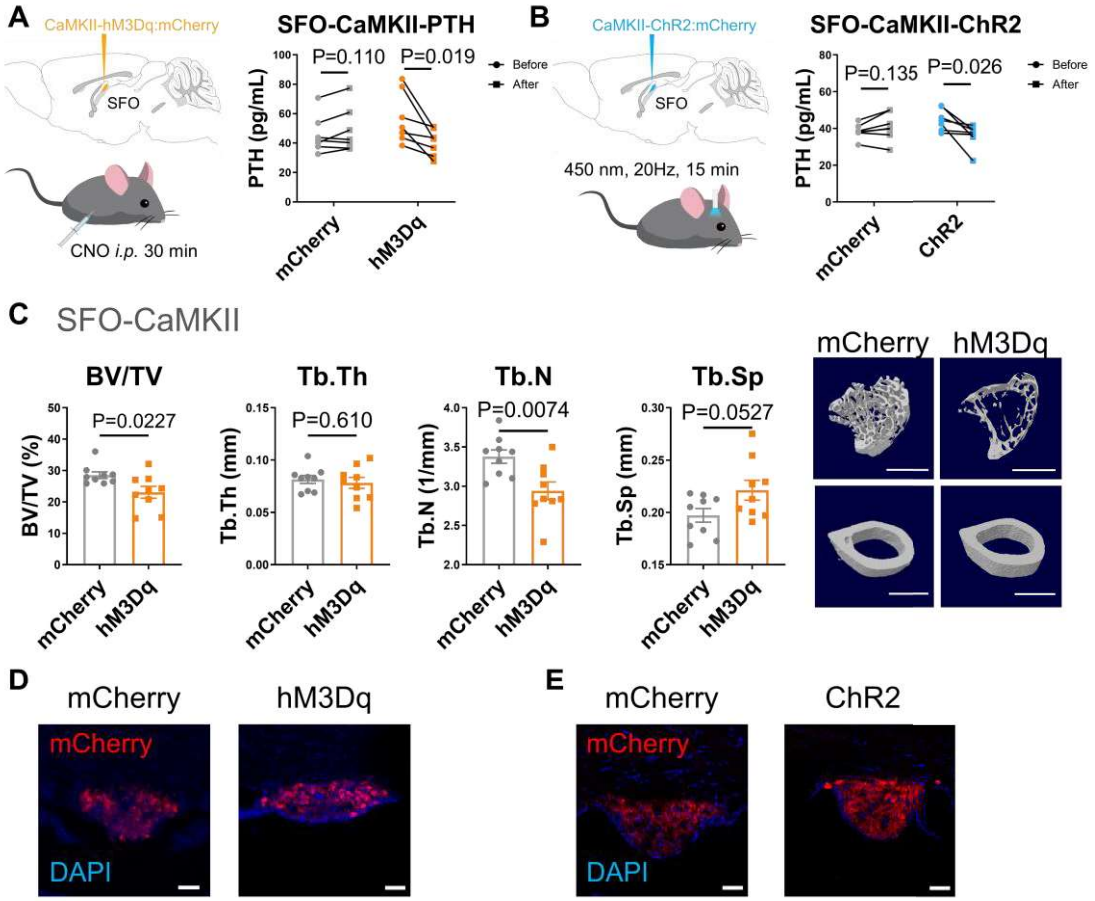

1107

1108 **Supplementary figure 4. Rapid serum PTH changes, bone phenotype and behavior**

1109 **analysis following stimulation of SFO^{CaMKII} neurons**

1110 **A,** Serum PTH changes after chemogenetic stimulation of CaMKII neurons (before and

1111 30 min after CNO *i.p.* injection) in SFO of C57 mice (n=7). **B,** Serum PTH changes

1112 after optogenetic stimulation of CaMKII neurons in SFO of C57 mice (n=6-7). **C,** Bone

1113 analysis after stimulation of SFO^{CaMKII} neurons. ***Left bar charts***, tibia trabecular percent

1114 bone volume (BV/TV), trabecular thickness (Tb.Th), trabecular number (Tb.N),

1115 trabecular separation (Tb.Sp) assessed by MicroCT (n=9 mice). ***Right***, 3D

1116 reconstruction of MicroCT analysis of tibia trabecular and femur cortical bones in

1117 hM3Dq and mCherry groups. Scale bar, 1 mm. **D,** The expression of hM3Dq-mCherry

1118 in CaMKII neurons in SFO. Scale bar, 50 μm. **E,** The expression of ChR2-mCherry in

1119 CaMKII neurons in SFO. Scale bar, 50 μm. P analyzed by paired two-tailed t-test in **A-**

1120 **B**; P analyzed by unpaired two-tailed t-test in **C**. All error bars and shaded areas show

1121 mean ± s.e.m.

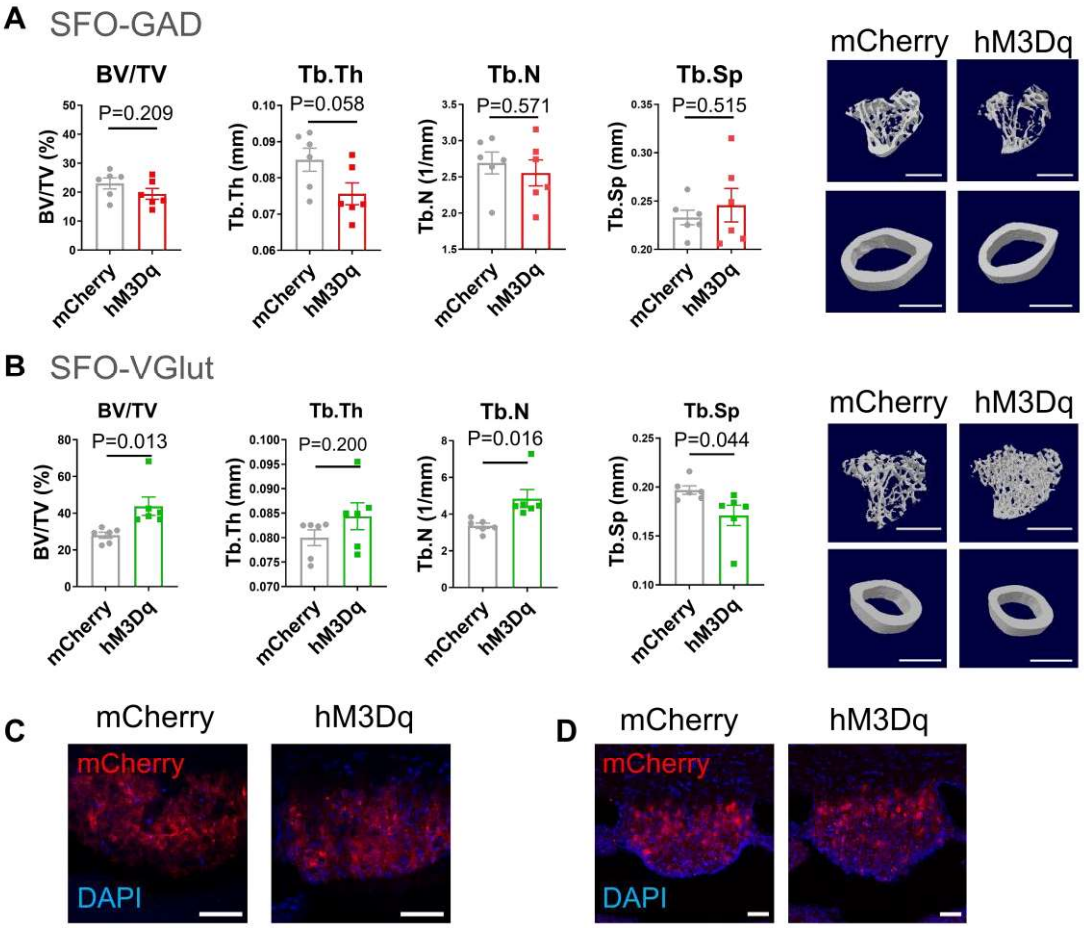

1122

1123 **Supplementary figure 5. Bone analysis following chemogenetic regulation of**

1124 **SFO^{GAD} and SFO^{VGlut} neurons**

1125 **A**, Bone analysis after chronic chemogenetic stimulation of SFO^{GAD} neurons for 4

1126 weeks. ***Left bar charts***, tibia trabecular percent bone volume (BV/TV), trabecular

1127 thickness (Tb.Th), trabecular number (Tb.N), trabecular separation (Tb.Sp) assessed by

1128 MicroCT analysis (n=6 mice). ***Right***, 3D reconstruction of MicroCT analysis of tibia

1129 trabecular and femur cortical bones in hM3Dq and mCherry groups. Scale bar, 1 mm.

1130 **B**, Bone analysis after chemogenetic stimulating SFO^{VGlut} neurons for 4 weeks. ***Left***

1131 ***bar charts***, tibia trabecular percent bone volume (BV/TV), trabecular thickness (Tb.Th),

1132 trabecular number (Tb.N), trabecular separation (Tb.Sp) assessed by MicroCT analysis

1133 (n=6 mice). ***Right***, 3D reconstruction of MicroCT analysis of tibia trabecular and femur

1134 cortical bones in hM3Dq and mCherry groups of VGlut2-cre mice. Scale bar, 1 mm. **C,**

1135 The expression of hM3Dq-mCherry in GABAergic neurons of SFO. Scale bar, 50 μm.

1136 **D,** The expression of hM3Dq-mCherry in glutamatergic neurons in SFO. of SFO. Scale

1137 bar, 50 μm. P analyzed by unpaired two-tailed t-test. All error bars and shaded areas

1138 show mean ± s.e.m.

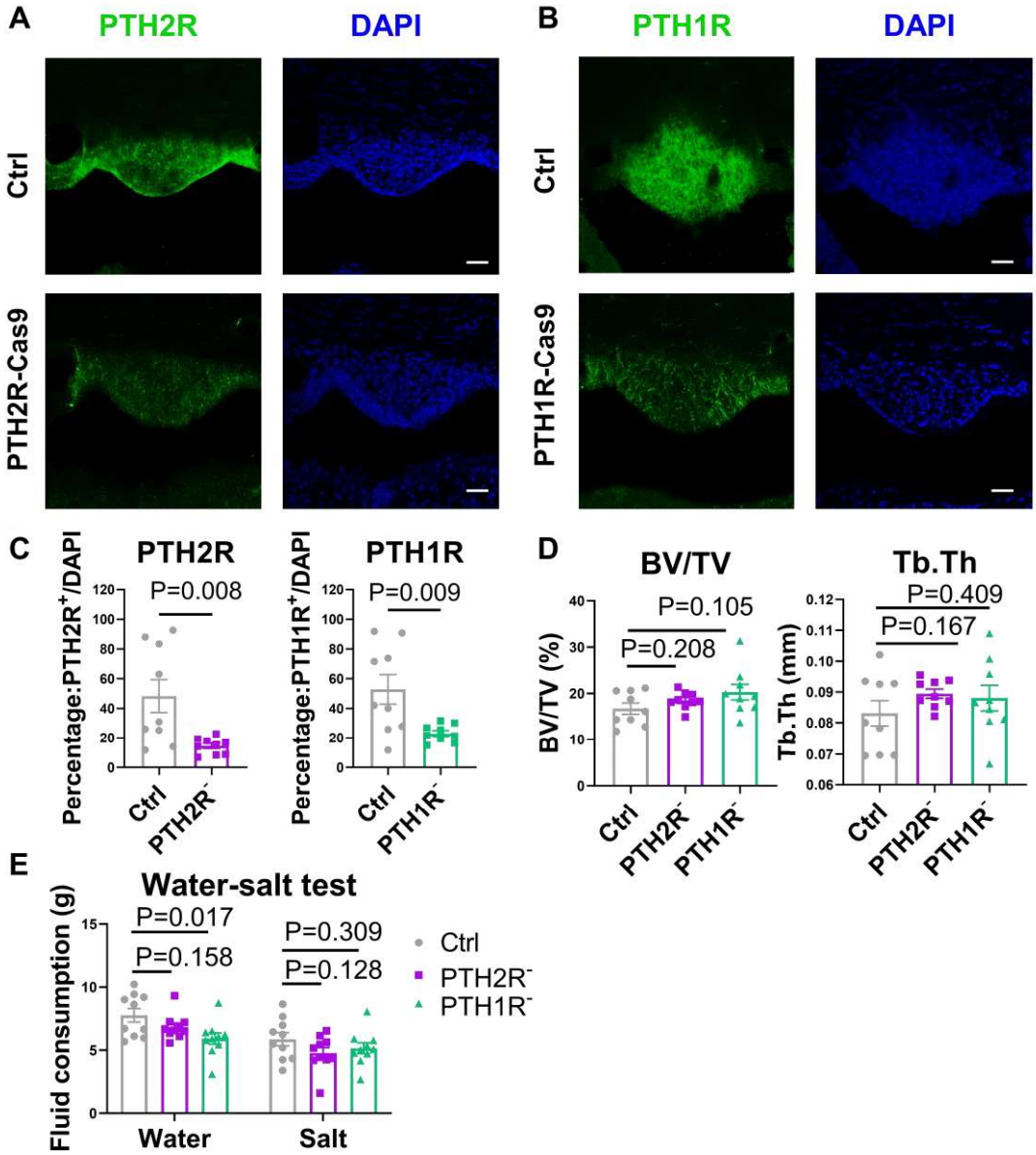

1139

1140 **Supplementary figure 6. Knockdown of PTH1R/PTH2R expression in SFO and**

1141 **related bone changes**

1142 **A**, Immunofluorescence staining of PTH2R in SFO of control and PTH2R knockdown
1143 mice. Scale bar, 50 μm. **B**, Immunofluorescence staining of PTH1R in SFO of control
1144 and PTH1R knockdown mice. Scale bar, 50 μm. **C**, Quantification of PTH2R/PTH1R
1145 positive cells in control and knockdown group (n=9 mice). **D**, Percentage of Bone
1146 volume (BV/TV), trabecular thickness (Tb.Th) of C57 mice tibia after knockdown of
1147 PTH1R/PTH2R (n=9 mice). **E,** Fluid consumption (water or 0.3M NaCl) tests in C57
1148 mice after knockdown of PTH1R/PTH2R expression in the SFO (n=9 mice). P
1149 analyzed using unpaired two-tailed t-tests. All error bars and shaded areas show mean
1150 ± s.e.m.

1151

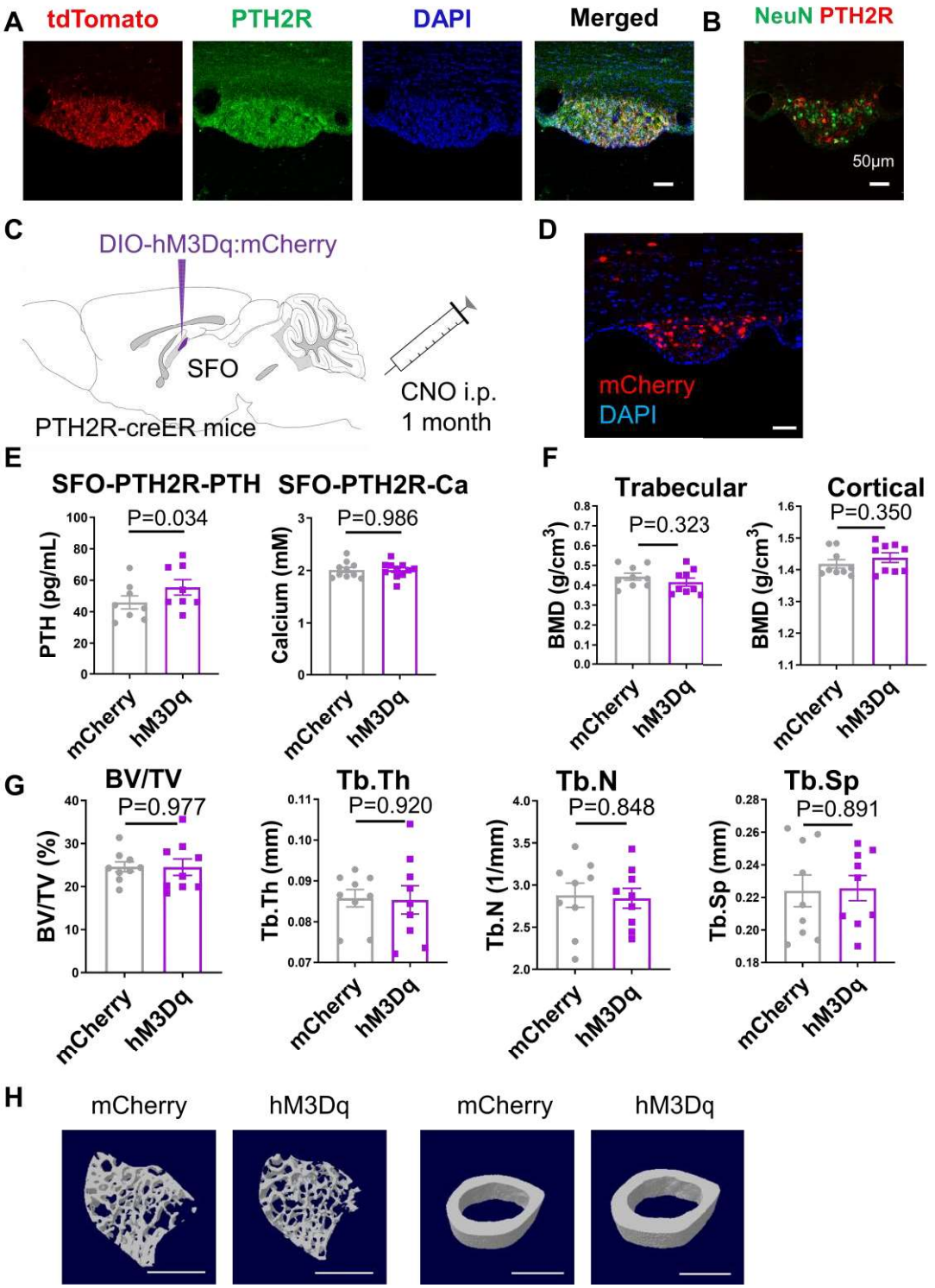

Supplementary figure 7 Serum PTH and bone metabolism changes after chemogenetic stimulation of SFO^{PTH2R} neurons in PTH2R-creER^{T2} mice.

A, Immunofluorescence (IF) staining of PTH2R colocalized with tdTomato signal in SFO of PTH2R-CreER^{T2} X Ai14 mice. Scale bar, 50 μm. **B**, PTH2R neurons labeled

1157 by AAV-DIO-mCherry transduction to the SFO of PTH2R-CreER^{T2} mice and
1158 colocalization with IF staining of NeuN (green). Scale bar, 50 μm. (**C-G**),
1159 Chemogenetic activation of PTH2R neurons in the SFO of PTH2R- CreER^{T2} mice
1160 (n=8-9 mice). **C**, Schematic showing injection of AAV-DIO-hM3Dq/mCherry into the
1161 SFO of PTH2R- CreER^{T2} mice followed with 1-month CNO *i.p.* administration. **D,**
1162 Expression of hM3Dq-mCherry within PTH2R neurons in SFO. Scale bar, 50 μm. **E,**
1163 Serum PTH, total calcium level of PTH2R-creER^{T2} mice after chemogenetic
1164 stimulation of SFO^{PTH2R} neurons. **F**, Tibia trabecular bone mineral density (BMD), and
1165 femur cortical BMD from MicroCT analysis of PTH2R-creER^{T2} mice after
1166 chemogenetic stimulation of SFO^{PTH2R} neurons. **G**, Percentage of bone volume
1167 (BV/TV), trabecular thickness (Tb.Th), trabecular numbers (Tb.N) and trabecular
1168 seperation (Tb.Sp) of PTH2R-creER^{T2} mice after chemogenetic stimulation of
1169 SFO^{PTH2R} neurons. **H**, 3D reconstruction of MicroCT analysis of tibia trabecular and
1170 femur cortical bones in mCherry and Hm3Dq groups. Scale bar, 1 mm. P analyzed using
1171 unpaired two-tailed t-test. All error bars and shaded areas show mean ± s.e.m.
1172

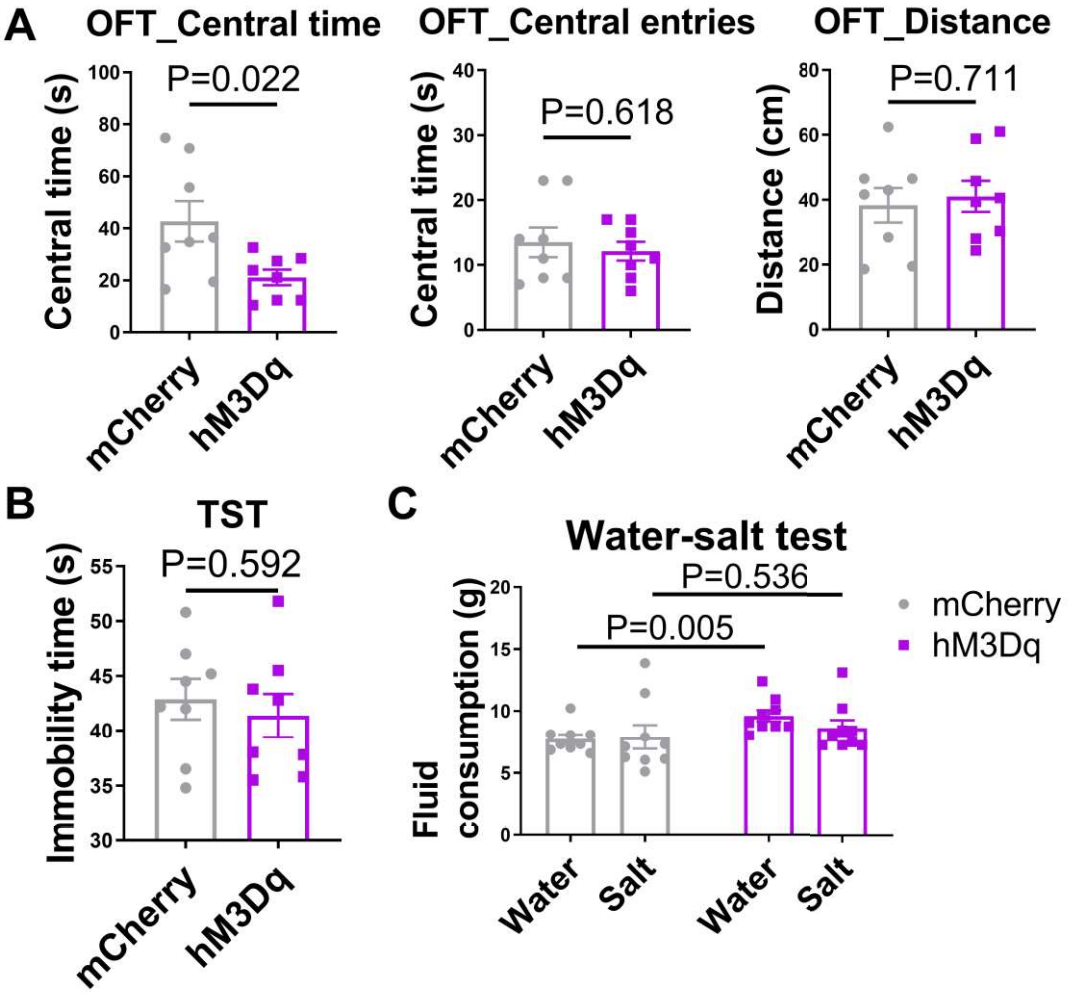

Supplementary figure 8 Behavior changes after chemogenetic stimulation of SFO^{PTH2R} neurons in PTH2R-creER^{T2} mice.

A, Time spent in center, central entries and total distance during open field test of PTH2R-creER^{T2} mice after chemogenetic stimulation of SFO^{PTH2R} neurons. (n=8 mice) **B**, Total immobility time during tail suspension test. (n=8 mice) **C**, Water and salt consumption of PTH2R-creER^{T2} mice after chemogenetic stimulation of SFO^{PTH2R} neurons. (n=8 mice) P analyzed using unpaired two-tailed t-test. All error bars and shaded areas show mean ± s.e.m.

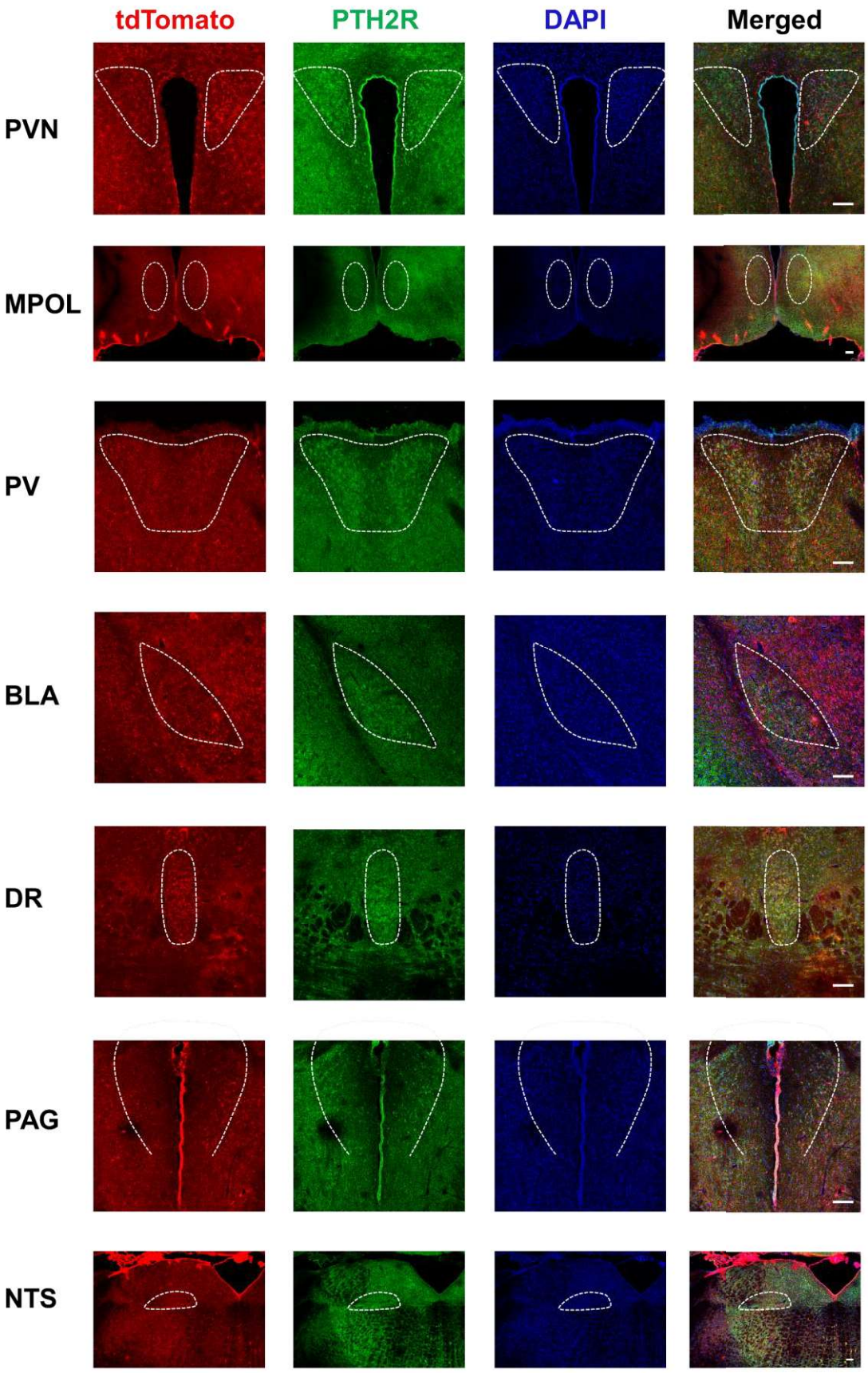

1182

1183 **Supplementary figure 9. Colocalization of immunofluorescence staining of PTH2R**

1184 **with tdTomato signals in PTH2R- CreER^{T2} X Ai14 mice brain.**

1185 Colocalization of immunofluorescence staining of PTH2R and tdTomato signals in
1186 PTH2R-creER^{T2} X Ai14 mice. PVN, paraventricular nucleus; MPOL, medial preoptic
1187 nucleus, lateral part; PV, periventricular nucleus; BLA, basolateral amygdala; DR,
1188 dorsal raphe; PAG, periaqueductal gray; NTS, nucleus of the solitary tract; Arc, arcuate
1189 nucleus. Scale bar, 100μm.

1190

1191

1192

1193

1194

1195

1196

1197

1198

1199

1200

1201

1202

1203

1204

1205

1206

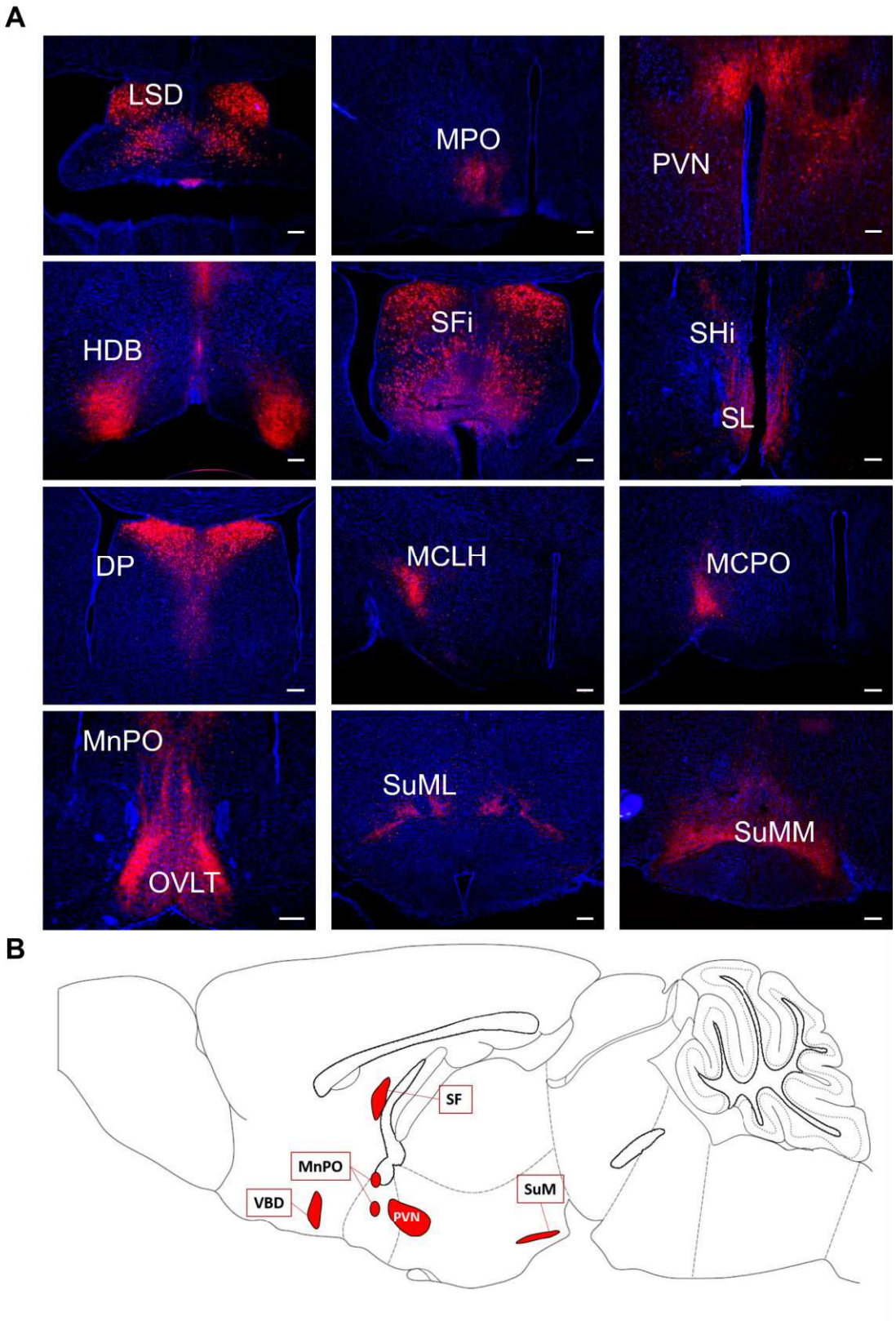

1207

1208 **Supplementary figure 10. Neural projections of SFO^{CaMKII} neurons into different**

1209 **brain nuclei in C57 mice.**

1210 **A**, SFO^{CaMKII} neurons labeled with AAV-CaMKII-mCherry project terminals into brain

1211 nuclei, including: the DP, dorsal peduncular cortex; HDB, nucleus of the horizontal
1212 limb of the diagonal band; LSD, lateral septal nucleus, dorsal part; MCLH,
1213 magnocellular nucleus of the lateral hypothalamus; MCPO, magnocellular preoptic
1214 nucleus; MnPO, median preoptic nucleus; MPO, medial preoptic nucleus; OVLT,
1215 vascular organ of lamina terminalis; PVN, paraventricular thalamic nucleus; SFi,
1216 septofimbrial nucleus; SHi, septohippocampal nucleus; SL, semilunar nucleus; SuML,
1217 supramammillary nucleus, lateral part; SuMM, supramammillary nucleus, medial part.
1218 Scale bar, 50μm **B**, Locations of brain nuclei receiving high density SFO^{CaMKII} neuronal
1219 projections (n=3 mice).
1220
1221
1222

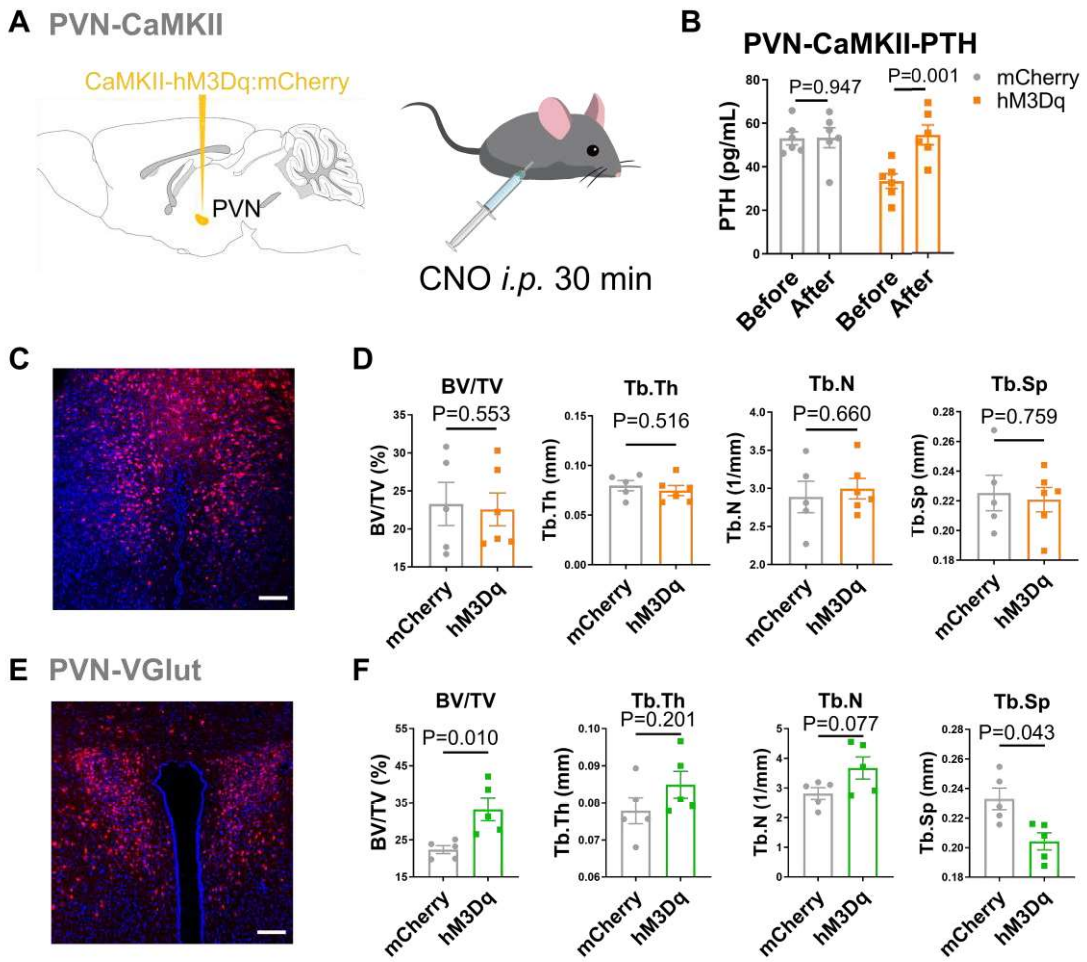

Supplementary figure 11. Serum PTH, bone structure and behavior changes after chemogenetic stimulation of PVN^{CaMKII} and PVN^{VGlut} neurons.

A, Schematic showing the injection of AAV-CaMKII-hM3Dq/mCherry in to PVN OF C57 mice and CNO administration. Serum are collected 30 min after CNO administration. **B,** Rapid Serum PTH changes after chemogenetic stimulation of CaMKII neurons (before and 30 min after CNO *i.p.* injection) in the PVN of C57 mice (n=5). **C,** Expression of hM3Dq-mCherry in CaMKII neurons in PVN. Scale bar, 100 μm. **D,** The tibia trabecular percent bone volume (BV/TV), trabecular thickness (Tb.Th), trabecular numbers (Tb.N), trabecular separation (Tb.Sp) assessed by MicroCT analysis after chemogenetic stimulation of PVN^{CaMKII} neurons for 1 month in C57 mice (n=5-6 mice). **E,** Expression of hM3Dq-mCherry in glutamatergic neurons

1235 in PVN. Scale bar, 100 μm. **F,** The tibia trabecular percent bone volume (BV/TV),
1236 trabecular thickness (Tb.Th), trabecular numbers (Tb.N), trabecular separation (Tb.Sp)
1237 assessed by MicroCT analysis after chemogenetic stimulation of PVN^{VGlut} neurons for
1238 1 month in VGlut2-cre mice (n=5 mice). P analyzed using unpaired two-tailed t-test.
1239 All error bars and shaded areas show mean ± s.e.m.

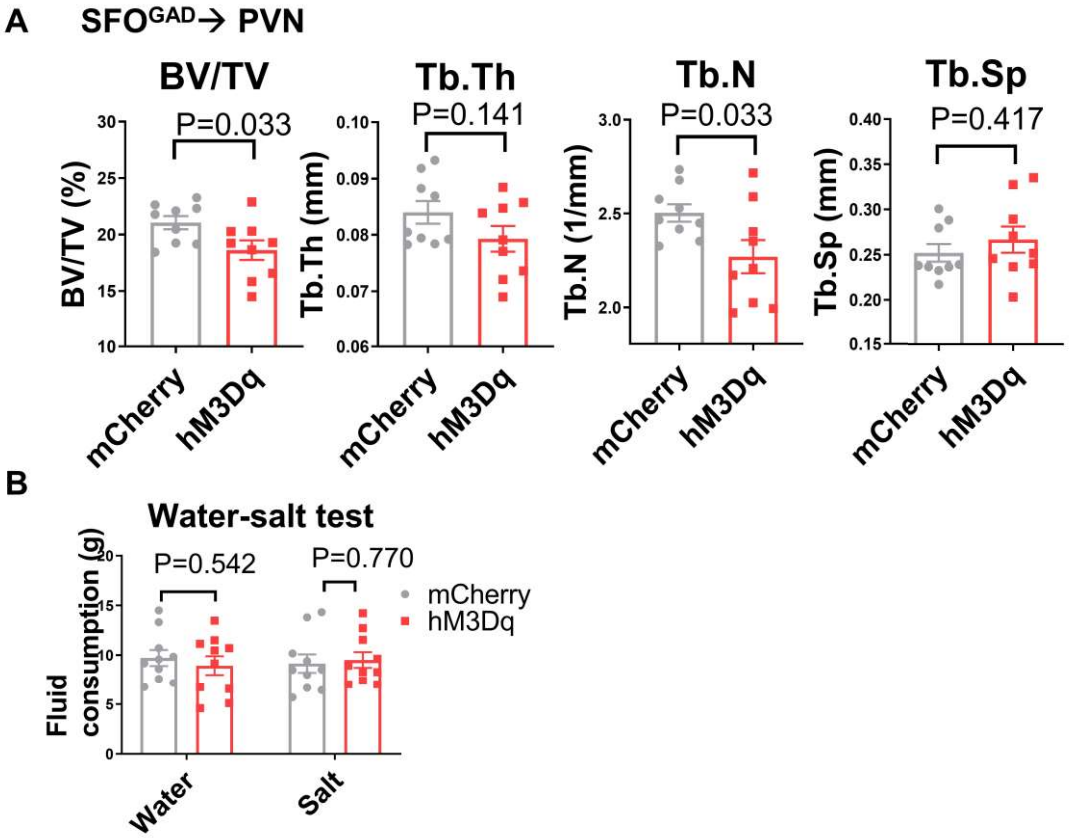

1240

1241 **Supplementary figure 12. Bone analysis and behavioral tests following stimulation**
1242 **of the SFO^{GAD}→PVN neural circuit**

1243 **A,** Tibia trabecular percent bone volume (BV/TV), trabecular thickness (Tb.Th),
1244 trabecular numbers (Tb.N), trabecular separation (Tb.Sp) assessed by MicroCT
1245 analysis after chemogenetic stimulation of SFO^{GAD}→PVN for 1 month in C57 mice
1246 (n=9 mice). **B,** Water and salt consumption of C57 mice after chemogenetic stimulation
1247 SFO^{GAD}→PVN for 1 month (n=10 mice). P analyzed using unpaired two-tailed t-test.
1248 All error bars and shaded areas show mean ± s.e.m.

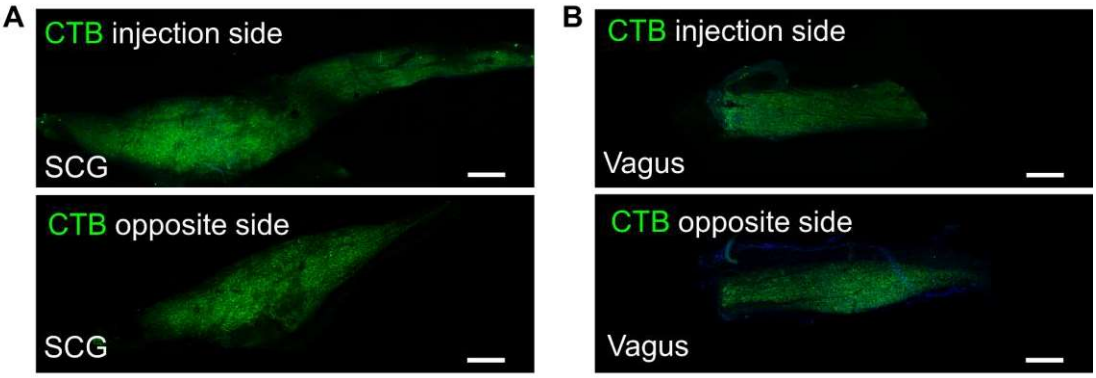

Supplementary figure 13. Neural specific retrograde tracing from rat parathyroid glands to upstream ganglia.

A, Choleral toxin B (CTB) signals observed in both the injection side and opposite side of sympathetic superior cervical ganglia (SCG). Scale bar, 500 μm. **B**, CTB signals observed in both the injection side and opposite side of sympathetic inferior vagus ganglia (Vagus). Scale bar, 500 μm.

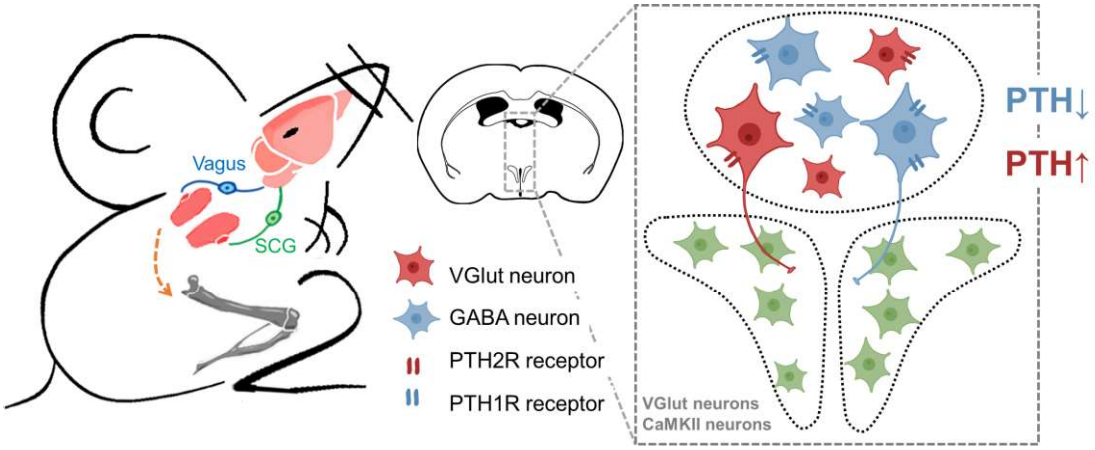

Supplementary figure 14.

Schematic summarizing the mechanism underlying the neural 2 regulation of PTH levels in the SFO and PVN. PTH, parathyroid hormone; PTH1R, parathyroid hormone receptor 1; PTH2R, parathyroid hormone receptor 2; SCG, superior cervical ganglia;

1264 VGlut, vesicular glutamate transporter; GABA, gamma-Aminobutyric acid.